

MICROCOPY RESOLUTION TEST CHART  
NATIONAL BUREAU OF STANDARDS-1963-A

12

AEOSR-TR- 82 - 1003

Final Technical Report

Air Force Office of Scientific Research

Grant Number <sup>AEOSR</sup> 177-3395

AD A121715

AN INVESTIGATION OF THE EFFECTS OF METALLURGICAL  
AND/OR TESTING VARIABLES ON THE ACOUSTIC EMISSION  
FROM CRYSTALLINE MATERIALS

- Submitted to -

Captain Steven G. Wax, Contract Monitor  
Electronic and Solid State Sciences  
Air Force Office of Scientific Research  
Building 410  
Bolling AFB, D.C. 20332

- Submitted by -

Professor Steve H. Carpenter  
Department of Physics  
University of Denver  
Denver, Colorado 80208

September, 1982

DTIC  
ELECTE  
NOV 22 1982  
S D  
E

DTIC FILE COPY

Approved for public release  
distribution unlimited.

Final Technical Report  
Air Force Office of Scientific Research  
Grant Number 77-3395

AN INVESTIGATION OF THE EFFECTS OF METALLURGICAL  
AND/OR TESTING VARIABLES ON THE ACOUSTIC EMISSION  
FROM CRYSTALLINE MATERIALS

- Submitted to -

Captain Steven G. Wax, Contract Monitor  
Electronic and Solid State Sciences  
Air Force Office of Scientific Research  
Building 410  
Bolling AFB, D.C. 20332

- Submitted by -

Professor Steve H. Carpenter  
Department of Physics  
University of Denver  
Denver, Colorado 80208

September, 1982

AIR FORCE OFFICE OF SCIENTIFIC RESEARCH (AFSC)  
NOTICE OF TRANSMITTAL TO DTIC  
This technical report has been reviewed and is  
approved for distribution under AFM 190-12.  
Distribution is unlimited.  
MATTHEW J. KENNER  
Chief, Technical Information Division

**UNCLASSIFIED**

REPORT DOCUMENTATION PAGE		READ INSTRUCTIONS BEFORE COMPLETING FORM
1. REPORT NUMBER <b>AFOSR-TR- 82-1003</b>	2. GOVT ACCESSION NO. <b>AD-A224775</b>	3. RECIPIENT'S CATALOG NUMBER
4. TITLE (and Subtitle) <b>AN INVESTIGATION OF THE EFFECTS OF METALLURGICAL AND/OR TESTING VARIABLES ON THE ACOUSTIC EMISSION FROM CRYSTALLINE MATERIALS</b>		5. TYPE OF REPORT & PERIOD COVERED <b>Final Technical Report 1 Aug. 1977 - 31 Jan. 1982</b>
7. AUTHOR(s) <b>Steve H. Carpenter</b>		6. PERFORMING ORG. REPORT NUMBER
8. CONTRACT OR GRANT NUMBER(s) <b>AFOSR 77-3395</b>		
9. PERFORMING ORGANIZATION NAME AND ADDRESS <b>Department of Physics University of Denver Denver, Colorado 80208</b>		10. PROGRAM ELEMENT, PROJECT, TASK AREA & WORK UNIT NUMBERS <b>2306-A2 6/102F</b>
11. CONTROLLING OFFICE NAME AND ADDRESS <b>Air Force Office of Scientific Research Building 410 Bolling AFB, Washington, D.C. 20332</b>		12. REPORT DATE <b>Sept. 1982</b>
14. MONITORING AGENCY NAME & ADDRESS (if different from Controlling Office)		13. NUMBER OF PAGES <b>80</b>
		15. SECURITY CLASS. (of this report) <b>Unclassified</b>
		15a. DECLASSIFICATION/DOWNGRADING SCHEDULE <b>N/A</b>
16. DISTRIBUTION STATEMENT (of this Report)  <b>Approved for public release; distribution unlimited</b>		
17. DISTRIBUTION STATEMENT (of the abstract entered in Block 20, if different from Report)		
18. SUPPLEMENTARY NOTES  <b>Program Manager: Steven G. Wax, Captain, USAF</b>		
19. KEY WORDS (Continue on reverse side if necessary and identify by block number) <b>Acoustic emission, plastic deformation, hexagonal close packed metals and alloys, precipitation hardenable alloys, dislocation mechanism deformation mechanisms, slip, twinning</b>		
20. ABSTRACT (Continue on reverse side if necessary and identify by block number)  <b>This is the final technical report for AFOSR Grant #77-3395, "An Investigation of the Effects of Metallurgical and/or Testing Variables on the Acoustic Emission from Crystalline Materials." The goal of this investigation was to characterize and correlate the acoustic emission measured during deformation with the responsible deformation mechanisms.</b>		

**UNCLASSIFIED**

**UNCLASSIFIED**

20. ABSTRACT continued

Two separate and distinct classes of materials have been investigated. The materials were chosen for the important fundamental information they could provide concerning the relationship between acoustic emission and the parameters involved and because of their practical importance to Air Force programs and objectives. The materials investigated were: one, a selection of precipitation strengthened metals and alloys, and two, a selection of metals and alloys having a hexagonal close packed structure. For both classes of materials the acoustic emission has measured during deformation for different metallurgical and testing parameters. The data have been analyzed and models and/or deformation mechanisms responsible for the measured emission have been identified.



Accession For	
NTIS GRA&I	<input checked="" type="checkbox"/>
DTIC TAB	<input type="checkbox"/>
Unannounced	<input type="checkbox"/>
Justification	
By	
Distribution/	
Availability Codes	
Dist	Avail and/or Special
<b>A</b>	



**UNCLASSIFIED**

## ABSTRACT

This is the final technical report for AFOSR Grant # 77-3395, "An Investigation of the Effects of Metallurgical and/or Testing Variables on the Acoustic Emission from Crystalline Materials." The goal of this investigation was to characterize and correlate the acoustic emission measured during deformation with the responsible deformation mechanisms. Two separate and distinct classes of materials have been investigated. The materials were chosen for the important fundamental information they could provide concerning the relationship between acoustic emission and the parameters involved and because of their practical importance to Air Force programs and objectives. The materials investigated were; one, a selection of precipitation strengthened metals and alloys and, two, a selection of metals and alloys having a hexagonal close packed structure. For both classes of materials the acoustic emission has measured during deformation for different metallurgical and testing parameters. The data have been analyzed and models and/or deformation mechanisms responsible for the measured emission have been identified.

## INTRODUCTION

This document is the Final Technical Report for AFOSR Grant #77-3395, "An Investigation of the Effects of Metallurgical and/or Test Variables on the Acoustic Emission from Crystalline Materials." Final results of the research activity during this program are reported on. The initial goal of the investigation has been to characterize and correlate the acoustic emission measured during deformation with the particular deformation mechanisms producing the emissions. Once this was accomplished the further goal was to determine and understand the effects of different metallurgical conditions and testing variables on the sources of the acoustic emissions and on the characteristics of the emissions produced.

The research activity and effort during the course of the grant have been divided into two separate but related studies on two distinct classes of materials. The materials investigated were: one, precipitation strengthened metals and alloys and, two, metals and alloys having a hexagonal close packed structure. Results from each investigation will be discussed in detail later in this report. However, for information a brief overview of each investigation is given below:

- 1) The acoustic emission generated during the plastic tensile deformation of a number of precipitation hardenable alloys has been investigated. A wide range of materials including several aluminum alloys and several austenitic stainless steels were tested. The alloys were selected both for their technical importance and to give a wide range of important metallurgical parameters such as stacking fault energy and elastic moduli. The acoustic emission generated during the deformation of these materials is characterized by a peak (Peak I) in acoustic emission near yield which is observed in all of the materials tested, and by a peak (Peak II) occurring at higher strains which is observed in some of the materials tested. This investigation has shown that peak I is caused by dislocation avalanche motion and the magnitude of the peak is primarily determined by the slip character of the material and the strength of the precipitates. It has been determined that peak II is caused by the fracture of inclusions within the metal matrix. This investigation

has been a joint effort with Dr. Clinton Heiple, Rockwell International, Rocky Flats Plant, Golden, Colorado. There has been a very close cooperation and interaction with Dr. Heiple during all phases of this investigation.

2) The acoustic emission generated during the deformation of a number of hexagonal close packed metals and alloys have been investigated. The materials were selected because of their complex deformation behavior and technical importance to the Air Force. The primary materials investigated were magnesium and titanium of which both pure metals and commercial alloys were tested. The anisotropic nature of these materials coupled with their complex deformation mechanisms produces a very complicated and unique acoustic emission which is sensitive to testing conditions, sample orientation, preferred orientation of the samples, thermal treatment and alloy chemistry. Dislocation slip and twinning have been identified as the major sources of acoustic emission. Dr. Mark Friesel carried out the majority of work in this particular investigation. Dr. Friesel used the results of this investigation for his doctoral thesis "Acoustic Emission from Magnesium and Titanium." Dr. Friesel is presently on the faculty of the Physics Department of the Colorado School of Mines.

## TECHNICAL DISCUSSION

The acoustic emission in both investigations was detected with a Dunegan-Endevco (D/E) S140 transducer, which is a PZT-5A piezoelectric, longitudinally resonant-type transducer with a 140 kHz resonant frequency. The transducer was located on the gage section of the samples and was coupled to the sample with a viscous resin (Dow 276-V9). The output of the transducer was amplified with a Panametrics Model 5050AE-160A preamplifier and amplified further with a D/E Model 301 totalizer with a frequency bandpass of 100-300 kHz. The amplified and bandpassed signal was measured with a Hewlett Packard 3400 A rms voltmeter. Amplitude distributions of the acoustic emission signals were determined after preamplification (60 dB gain) with a D/E 920 Distribution Module. Near the end of the investigations, a Nicolet Explorer III digital oscilloscope was obtained. Traces of the acoustic emission signal after preamplification were obtained at several strains for a few samples.

Deformation was produced with a universal testing machine, having a screw-driven crosshead, at various constant crosshead speeds. The load on the sample was obtained from the testing machine load cell. Sample deformation was measured with a extensometer attached to the gage section.

The tensile bars used for most of the tests had a circular cross section of 4 mm diameter with a 19 mm reduced section and threaded ends. This tensile bar is one of the small-size round tension test specimens proportional to the standard round specimen (see Figure 8 of ASTM, 1979). The grips of all samples were preloaded to at least 150 percent of the expected ultimate load before testing in order to minimize acoustic emission from the grips during the actual test. Typical compression samples were cylinders with a gage length of 1 inch and a 3/8 inch diameter. A flat, machined to a depth of less than 0.01 inch into the side of the cylinder served as a mounting surface for the transducer. For some materials smaller rectangular samples were used.

## I. Investigation of the Acoustic Emission Generated During the Plastic Deformation of a Selection of Precipitation Strengthened Alloys

The acoustic emission generated during the plastic deformation as a function of prior heat treatment for a wide range of precipitation hardenable alloys has been investigated in detail. The alloys investigated were chosen for their practical importance and to give a wide range of important metallurgical parameters. The alloys investigated included aluminum alloys 7075, 6061, 2219; austenitic stainless steels JBK-75 (an alloy similar to A286) and KHB (an experimental alloy age-hardened with a NiBe precipitate); along with Incoloy 903, 17-10P and sterling silver. As reported in our first annual technical report, it is possible to observe completely divergent behavior in the acoustic emission as a function of heat treatment for different alloys. For example, 2024 aluminum alloy has a minimum amount of acoustic emission (measured at yield) when heat treated for maximum hardness. Conversely, JBK-75, an austenitic stainless steel which is also a precipitation hardenable alloy has a maximum acoustic emission when heat treated for maximum strength.

The acoustic emission in terms of the rms voltage and stress are shown as a function of strain in Fig. 1 for a 7075 aluminum sample. Two distinct acoustic emission peaks are clearly shown for this material and heat treatment. The acoustic emission measured from all of the alloys tested went through a maximum or peak (Peak I) near the elastic yield, similar to the one shown in Fig. 1. The second peak (Peak II) which is observed at higher strain was found to occur in some alloys tested and to be totally absent in others.

The initial goal of this investigation was to determine the source of the peak I acoustic emission. The height of the rms voltage at the maximum of peak I was determined for a series of heat treatments. The location of peak I coupled with the absence of twinning in these materials strongly suggested that the acoustic emission was due to some type of dislocation process. The question that needed to be answered was how do the precipitates in these materials effect the dislocation motion and the acoustic emission it produces.

Our investigation has shown that the acoustic emission at peak I is produced by dislocation avalanches which are primarily determined by the slip character of the material and by the size and strength of the precipitates. In alloys where cross slip is relatively easy, dislocations pass precipitates by cross slipping around them individually, a process unlikely to lead to dislocation avalanches. Ease of cross slip is governed mainly by the separation of partial dislocations, which is in turn directly proportional to the elastic modulus and inversely proportional to the stacking fault energy. It is important to understand that slip is governed by both the stacking fault energy and the modulus. In easy cross slip systems (high stacking fault energy, low modulus), acoustic emission should be relatively low after aging and not very sensitive to the size or strength of the precipitates achieved during aging. Precipitation strengthened aluminum alloys fall in this class.

By contrast, in alloys where cross slip is more difficult, dislocations tend to pile up at precipitates and—if the precipitates are not too strong—cut through them in a way more likely to produce avalanche motion. In these systems (low stacking fault energy, high modulus) the acoustic emission levels may be relatively high after aging and sensitive to the size and nature of the precipitates. In particular, the amount of acoustic emission observed near yield should increase with increased aging time until the precipitates become strong enough so that they begin to no longer serve as breakable pins, at which point the amount of acoustic emission generated should decrease. Precipitation strengthened austenitic stainless steels fall in this class.

If the breakable pins are Cottrell atmospheres instead of precipitates, then slip character should have little effect on the amount of acoustic emission produced. Cottrell atmospheres are known to provide breakable pinning of dislocations under certain conditions, as for example when Portevin-LeChatelier (serrated) yielding occurs or in many cases when load drops are produced at yield. Substantial acoustic emission would therefore be expected in both easy and difficult cross slip systems when yield points or serrated yielding is observed. Furthermore, precipitation removes material from solid solution, thus, acoustic emission may be reduced during

aging in some systems simply by reducing the pinning of dislocations by Cottrell atmospheres. A flow chart schematic showing the model developed during this investigation is given in Fig. 2.

A sizable amount of experimental data was generated from a number of alloys having a wide variation of slip character, i.e., stacking fault energy and modulus. The data agreed with the model discussed above very well. A summary is shown in Fig. 3.

Results from this portion of the investigation were presented at an International Meeting on "Elastic Waves and Microstructure," University of Oxford, Great Britain, December 1980. The presentation was then published as a portion of the conference proceedings in the Nov.-Dec. 1981 (Vol. 15) issue of Metal Science. A copy of this publication is attached if further detail is desired.

In addition to studying the acoustic emission at yield (Peak I), the location of peak II, as a function of heat treatment and other characteristics of peak II have been investigated.

The height of peak II in 7075 Al is essentially independent of heat treatment, as shown in Fig. 4. The response of peak I to heat treatment is also shown in Fig. 4 for comparison. The stress and plastic strain at which peak II occurred in 7075 are shown in Fig. 5.

The acoustic emission in peak II has been shown to arise in 7075 aluminum from the fracture and/or decohesion of inclusions (Carpenter and Higgins, 1977; Hamstad and Mukherjee, 1975; Cousland and Scala, 1981). In much of the literature the proposed mechanism to explain the acoustic emission at peak II is stated as the fracture and/or debonding of inclusions and/or precipitates. It should be made clear that these are not the precipitates used to harden or strengthen the material but are much larger impurity type inclusions. Evidence supporting this conclusion includes the observations that peak II essentially disappears in compression, that no internal friction peak is associated with peak II while there is an internal friction peak concurrent with peak I, and that peak II only occurs after significant plastic strain.

McBride, et al., 1981, have recently investigated acoustic emission during slow crack growth in 7075 Al. They found quantitative agreement between the amplitude distribution of the burst acoustic emissions and the area size distribution of the large intermetallic inclusions in the alloy.

When high purity material without these inclusions was tested, no burst emission was observed. Furthermore, when the alloy was in the "0" condition, no burst emission was observed either. In the latter case, inclusions on the fracture face were unbroken. These observations indicate the emission is associated with inclusion fracture rather than debonding.

Our observations on the behavior of peak II with heat treatment are consistent with the peak arising from inclusion fracture during deformation. For the three alloys in which peak II was definitely observed, the plastic strain at the peak II maximum was lowest for the maximum-strength aging condition. (The stress at which the peak II maximum occurred was correspondingly closest to the yield stress for the maximum-strength aging condition.) The data are consistent with the view that a substantial local stress, greater than the yield stress even in the maximum-strength aging condition, is required to fracture the inclusions in these alloys. The required local stress is achieved by a combination of the average applied stress and the stress concentration resulting from plastic flow. Thus, less plastic flow is required to achieve particle fracture in the maximum-strength condition, as observed. If the matrix is sufficiently soft, then a stress high enough to cause general particle failure cannot be achieved and no peak II occurs.

During deformation, the stress on an inclusion differs from the stress in the matrix because of a difference in elastic moduli between matrix and inclusion (inhomogeneity stress), because of accommodation stresses between the inclusion which is assumed to only deform elastically and the plastically deforming matrix (plasticity stress) and because of different thermal expansion coefficients of inclusion and matrix (misfit stress).

A rough calculation of the stress on the inclusions at the peak II maximum for various heat treatments of 7075 Al can be made on the basis of the work of Shibata and Ono (1978a,b) and Coade et al., 1981. The inclusions in commercial 7075 Al are complex intermetallics with either Si or Fe as the major constituent and probably containing substantial oxygen (El Soudani, 1973). To the best of our knowledge, Young's moduli of these inclusions have not been determined, but they probably lie in the range of a borosilicate glass (50-70 GPa; Anon, 1967),  $\text{Cu}_3\text{Al}$  (81 GPa; Guillet and LeRoux, 1967),  $\text{Al}_2\text{Cu}$  (95 GPa, Guillet and LeRoux, 1967), and FeO (145 GPa - calculated from a shear modulus of 54 GPa [Jackson et al., 1978] assuming Poisson's ratio to be equal to 1/3).

If it is assumed that the plasticity stress is proportional to  $\epsilon_p^2$  as observed by Coade et al. (1981), up to 0.5 percent plastic strain and is linear with  $\epsilon_p$  thereafter (with the slope at 0.5 percent plastic strain) and furthermore that the proportionality constant ( $1.6 \times 10^6$  MPa) is the same in 7075 Al as that found for spherical silicon particles in Al-Si-Mg alloy, then the plasticity stress can be estimated. The estimated plasticity stresses at the matrix strains corresponding to peak II are tabulated in Table 1.

Table 1

Estimated Stress (MPa) on Inclusions at Peak II Maximum, 7075 Al

<u>Heat Treatment</u>	<u>Yield Stress</u>	<u>Peak II Stress</u>	<u><math>\epsilon_p</math> Peak II (%)</u>	<u>Misfit Stress</u>	<u>Inhomo- genity Stress</u>	<u>Plas- ticity Stress</u>	<u>Total Stress</u>
Solution treated, Quenched	180	275	3.2	-180	410	470	700
1 hr 250°C	490	545	2.2	-490	820	310	640
8 hr 250°C	535	570	1.7	-535	855	230	550
25 hr 250°C	555	580	1.2	-555	870	150	465
8 hr 350°C	405	445	1.6	-405	670	220	485

The total estimated stress on the inclusions at the peak II maximum is roughly the same for all heat treatments, as expected if the acoustic emission peak arises from inclusion fracture. The observations that the height of peak II was independent of heat treatment and that no large shifts occurred with heat treatment in the acoustic emission signal amplitude distributions are also consistent with the inclusion fracture strength being insensitive to aging treatment.

The other observation on peak II was that the amplitude distribution contained a higher fraction of high amplitude events than peak I. This difference is consistent with the two peaks arising from different mechanisms.

Results from this portion of the investigation will be reported on at the 6th International Acoustic Emission Symposium in Japan, October 1982. A comprehensive paper has also been prepared which has been submitted to the

Journal of Acoustic Emission for publication. A copy of this paper is attached to this report.

The investigation of acoustic emission from precipitation strengthened alloys was a joint effort with Dr. Clinton Heiple, Rockwell International, Rocky Flats Plant, Golden, Colorado. The close association and working relationship has been most beneficial.

#### Bibliography

- S.H. Carpenter and F.P. Higgins (1977) Metall. Trans. A, 8A, 1629-32.
- R.W. Coade, J.R. Griffiths, and B.A. Parker (1981) Philos. Mag. A, 44, 357-372.
- S. Mck Cousland and C.M. Scala (1981) Met. Sci, 15, 609-614.
- S.M. El-Soudani and R.M. Pelloux (1973) Metallography 6, 37-64.
- L. Guillet and R. LeRoux (1967) Intermetallic Compounds, ed. J.H. Westbrook, Wiley, New York, p. 456.
- M.A. Hamstad and A.K. Mukherjee (1975) "A Comparison of the Acoustic Emission Generated by Tensile and Compression Testing of 7075 Aluminum," UCRL-77502, Lawrence Livermore National Laboratory, Livermore, November [D 676].
- I. Jackson, R.C Liebermann, and A.E. Ringwood (1978) Phys. Chem. Minerals 3, 11-31.
- M. Shibata and K. Ono (1978a) Mater. Sci. & Eng. 34, 131-137.
- M. Shibata and K. Ono (1978b) Acta Metall. 26, 921-932.

## II. Investigation of the Acoustic Emission Generated During the Deformation of Hexagonal Close Packed Metals and Alloys

The acoustic emission generated during deformation has been studied in detail for a number of different hexagonal close packed (hcp) metals and alloys. Materials selected were chosen to give a range of hexagonal metals and alloys of interest to the United States Air Force. The primary materials investigated were pure and commercial alloys of magnesium and titanium. Hexagonal close packed metals are generally anisotropic with complex deformation modes and/or mechanisms. The acoustic emission generated depends strongly on the metallurgical variables such as preferred orientation, thermal history, purity, etc., as well as on the testing variables (see previous annual reports). The goals of this particular investigation were: one, to identify and correlate the acoustic emission generated with particular sources operable during deformation, and two, to determine how various testing and metallurgical variables effect both the operation of the sources producing the acoustic emission and the characteristics of the emissions themselves.

The most striking feature of acoustic emission from the hexagonal close packed materials is the strong dependence and unique pattern of acoustic emission for a particular set of metallurgical and testing conditions. Figures 6 and 7 show the acoustic emission parameters and load for AZ31B magnesium tooling plate tested in compression. The only difference in these two tests is the orientation of the sample. Data in Fig. 6 were generated with a sample whose compression axis was normal to the plane of the plate. Data in Fig. 7 were generated using a sample whose compression axis was parallel to the plane of the plate. The differences in the data are truly remarkable and are due to a preferred orientation in the plate. Comparison of x-ray surface diffraction with that from magnesium powder indicated a strong preferred orientation in the AZ31B plate. It was found that the normal to the basal plane tended to be perpendicular to the plate surface. Wide variations in the acoustic emission from titanium and its alloys were also observed as were demonstrated in the second annual technical report. Figure 8 shows acoustic emission measured in terms of rms voltage along with the load as a function of time for a relatively pure (50A) titanium sample tested in tension. The acoustic emission at yield has been

identified as due to dislocation slip processes (most likely dislocation avalanche motion) while the acoustic emission at higher strains has been shown to be due to twin nucleation (see second annual technical report for detail and confirming micrographs). For comparison Fig. 9 shows the acoustic emission from a tension test of Ti-6AL-6V-2SN. This alloy was specifically designed to minimize twinning and none is observed. As shown in Fig. 9 the only acoustic emission is a slight acoustic emission peak observed at yield (rms voltage scales are the same in both figures).

In all cases investigated the acoustic emission generated during deformation was found to be consistent with dislocation slip and/or deformation twinning mechanisms.

The acoustic emission due to dislocation slip mechanisms was found only at yield, when serrated yielding was observed or when there was a significant hardening or stress step in the stress strain curve. The acoustic emission from the dislocation slip mechanisms was characterized by being continuous in nature, having a relatively low energy per event when compared to the acoustic emission from twinning and generally having lower amplitude signals. The emission from the dislocation slip could be well characterized in its strain rate behavior. The data from dislocation mechanisms in all cases was consistent with the expression

$$V_{\text{rms}} \propto \dot{\epsilon}^{\frac{1}{2}}$$

where  $V_{\text{rms}}$  is the rms voltage of the emission and  $\dot{\epsilon}$  is the strain rate of the deformation test. The acoustic emission from dislocation slip at yield was found to be sensitive to material purity and thermal treatment. In ultra pure materials little or no emission at yield was observed, even though extensive slip took place. As the impurity level was increased, providing pinning and/or locking of the dislocation lines, the emission was found to increase. The more the slip was consistent with a dislocation avalanche or breakaway process the higher the acoustic emission at yield. In a similar manner thermal treatments which provided dislocation pinning gave higher acoustic emission. For example a slow or furnace cool, one which allowed impurities to move to the dislocation lines and render them immobile, produced significantly higher acoustic emission than a rapid cool or quench which essentially froze the impurities in solid solution.

The acoustic emission from twinning can be characterized as being more burst-like in nature, having a higher energy per event and in general having a higher amplitude signal. In various test materials twinning was found to occur at different stress-strain levels. Acoustic emission from twinning was observed in the elastic range (see figure 6). In this data from AZ31B magnesium plate the first rms voltage maximum has been clearly identified by metallography and other means as due to twin nucleation. Notice that it occurs early in the elastic region, in fact, the instant that any load is applied to this material in this orientation acoustic emission from twinning is observed. However, as shown in Fig. 8 the acoustic emission for twinning in this material (50A titanium) occurs at strains well past yield.

Some very unique acoustic emission behavior can be observed in samples oriented to take advantage of particular deformation mechanisms. Figure 10 shows the temperature dependence of the critical resolved shear stresses for slip and the activation stresses for twinning in titanium. The subscript, s, refers to slip and the subscript, t, refers to twinning.

Figure 11 shows acoustic emission data for a VP\* titanium sample tested in tension. Note that there is a small amount of acoustic emission beginning at yield but the majority is a burst type of emission at higher strains. Due to the preferred orientation of the sample material it was determined that  $\{11\bar{2}2\}$  twinning should be capable of accommodating the strain imposed during loading. Figure 10 has shown that the critical stress for activation of  $\{11\bar{2}2\}$  twinning decreases significantly with temperature. If the magnitude of the acoustic emission from this mode of twinning is related to stress necessary to activate the twin, one would expect a decrease in the magnitude of the acoustic emission, a decrease in the energy per event and a shift of the maximum to lower strains as the temperature is lowered. Figures 12 and 13 provide acoustic emission data showing that this is exactly what occurs. Possibly more surprising is that due to the complementary nature of temperature and strain rate one would expect in this case a decrease in acoustic emission with increasing strain rate.

---

\* VP trademark Materials Research Corp.

Figure 14 shows data confirming the expected behavior. This is the only case to the author's knowledge of decreasing acoustic emission with increasing strain rate.

In general one may state that the acoustic emission generated from hexagonal close packed materials is due to dislocation slip processes, twin nucleation and possibly twin growth. Acoustic emission from dislocation slip processes will depend on sufficient dislocation avalanche motion. It is characterized by being continuous or near continuous, having a low energy per event ratio and having a low signal amplitude. Emissions from this type of a source are generally observed at yield, when serrated yielding occurs or when there is significant hardening or stress steps in the stress strain curve. It should be pointed out in many cases slip can occur without significant or measurable acoustic emission being generated. Acoustic emission from twinning is more burst-like in character, has a higher energy per event and can, depending on the material, be found anywhere in the stress strain curve. It has been our experience that whenever twinning occurs acoustic emission is generated. As stated earlier in the Second Annual Report, acoustic emission measurements may be the most sensitive technique available to establish the stress-strain necessary to activate a particular twinning system.

Dr. Mark Friesel has completed a doctoral dissertation from research carried out in the portion of the program. The dissertation was defended by Dr. Friesel and accepted by the Physics Department of the University of Denver. The title is "Acoustic Emission in Magnesium and Titanium." Dr. Friesel is currently employed by the Physics Department of the Colorado School of Mines. Three publications are currently being prepared from the data generated during the investigation on hexagonal close packed metals and alloys. They are: one, a paper on acoustic emission from magnesium, two, a paper on acoustic emission from titanium, and three, a paper on unique acoustic emission results in hexagonal close packed metals and alloys.

SHC:cg

10-7-82

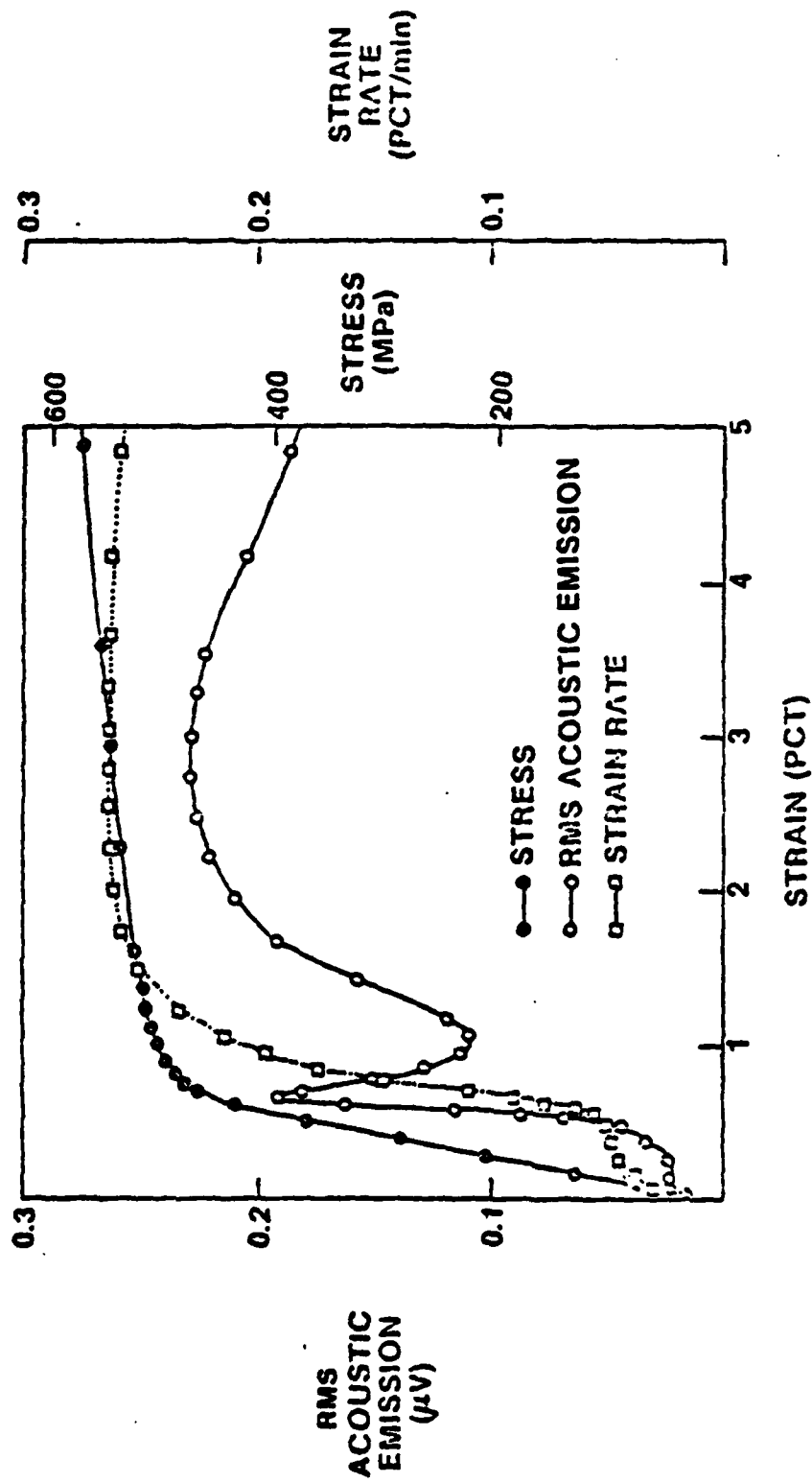


Figure 1. Acoustic emission measured by rms voltage, stress and strain rate for a 7075 aluminum tensile test aged one at 120°C. Both peaks in the acoustic emission are clearly shown.

SOLID SOLUTION STRENGTHENED

PRECIPITATION STRENGTHENED

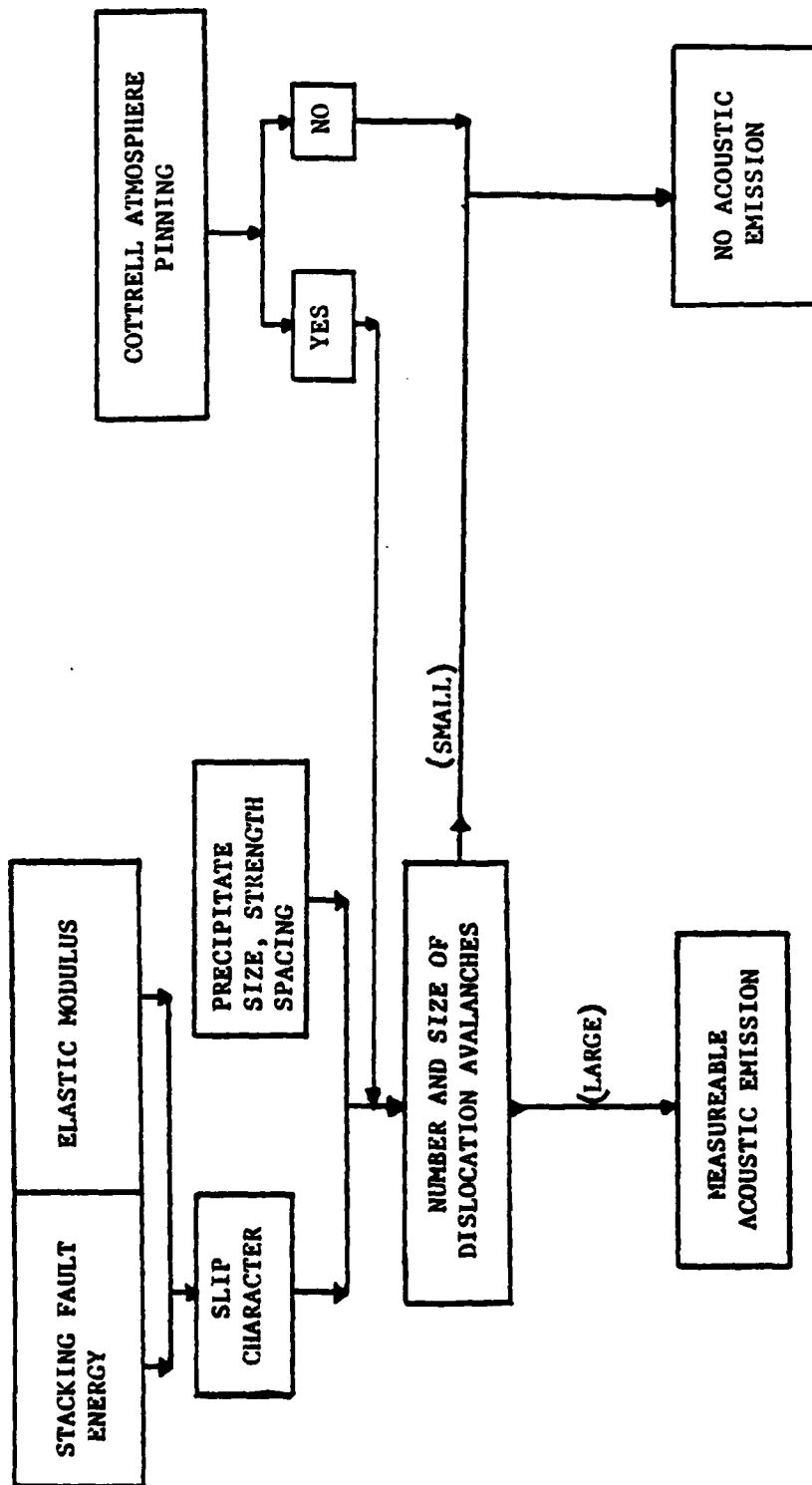


Figure 2. Schematic of model proposed to explain acoustic emission from precipitation strengthened metals and alloys.

ALLOY	SLIP CHARACTER	HEAT TREATMENT, CONDITION FOR MAXIMUM A.E.	A. E. INCREASE WITH INITIAL AGEING?	PRECIPITATION STRENGTHENED	HARDENING PRECIPITATE AT MAXIMUM A.E.	PRECIPITATE CUTTABLE	MAXIMUM RMS VOLTAGE ( $\mu$ V)
2219	EASY	T4 (SOLUTIONIZED NOT TESTED)	NO	YES	GP (1)	YES	0.25
6061	CROSS	SOLUTIONIZED & QUENCHED	NO	YES	NONE	—	0.20
7075	SLIP	SOLUTIONIZED & QUENCHED	NO	YES	NONE	—	0.67
Ag-7ZCu		SOLUTIONIZED & QUENCHED	NO	YES	NONE	—	0.03
5083		"0"	—	NO	—	—	40.0
JBK-75	MODERATELY DIFFICULT	UNDERAGE	YES	YES	$\delta'$	YES	2-3
KH8	CROSS	UNDERAGE	YES	YES	GP ZONES	YES (?)	0.3
INCALLOY 900	SLIP	SLIGHT OVER-AGE	YES	YES	$\delta'$	YES	6.0
17-10P	DIFFICULT CROSS SLIP	NO. A.E. PEAK	—	YES	M <sub>23</sub> C <sub>6</sub>	NO	—

Figure 3. Tabular listing of experimental data showing agreement with proposed model.

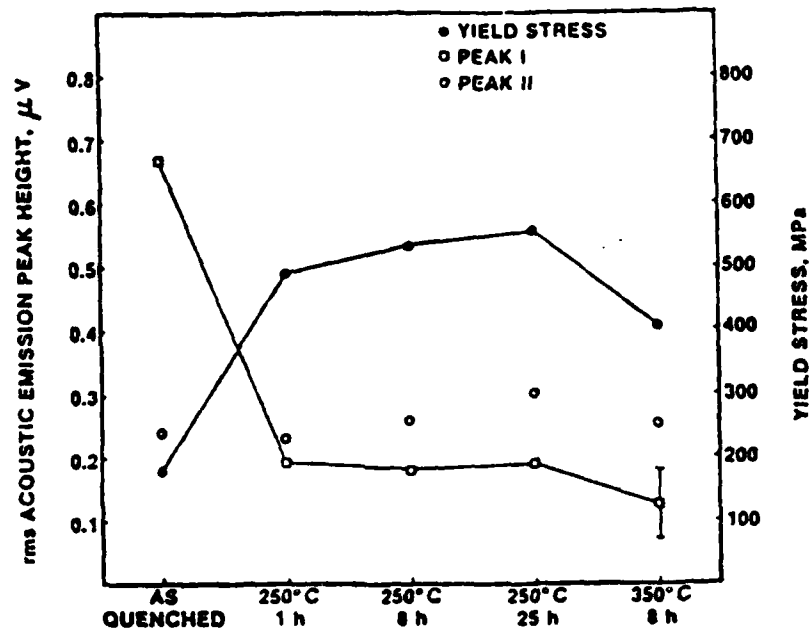


Figure 4. Heights of acoustic emission peaks I and II in terms of rms voltage, and yield stress, for 7075 aluminum tested in tension as a function of heat treatment.

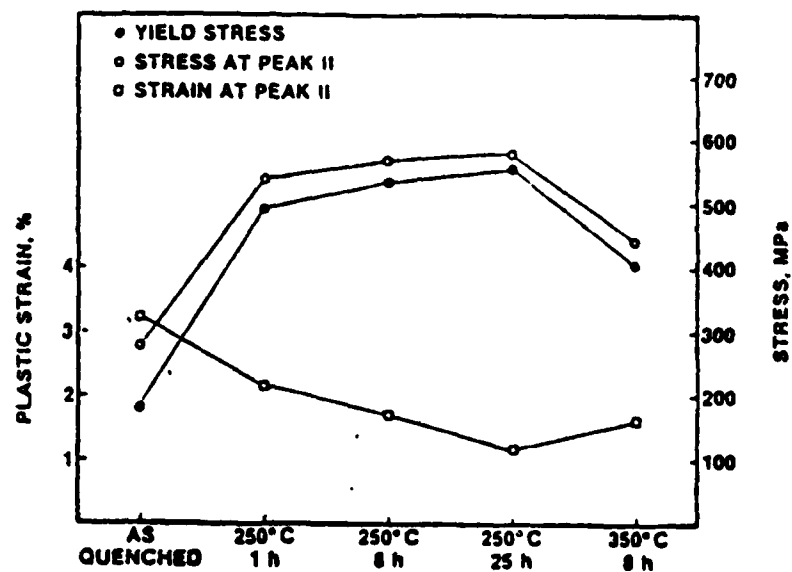


Figure 5. Stress and plastic strain at the acoustic emission peak II maximum, and yield stress, for 7075 aluminum tested in tension as a function of heat treatment.

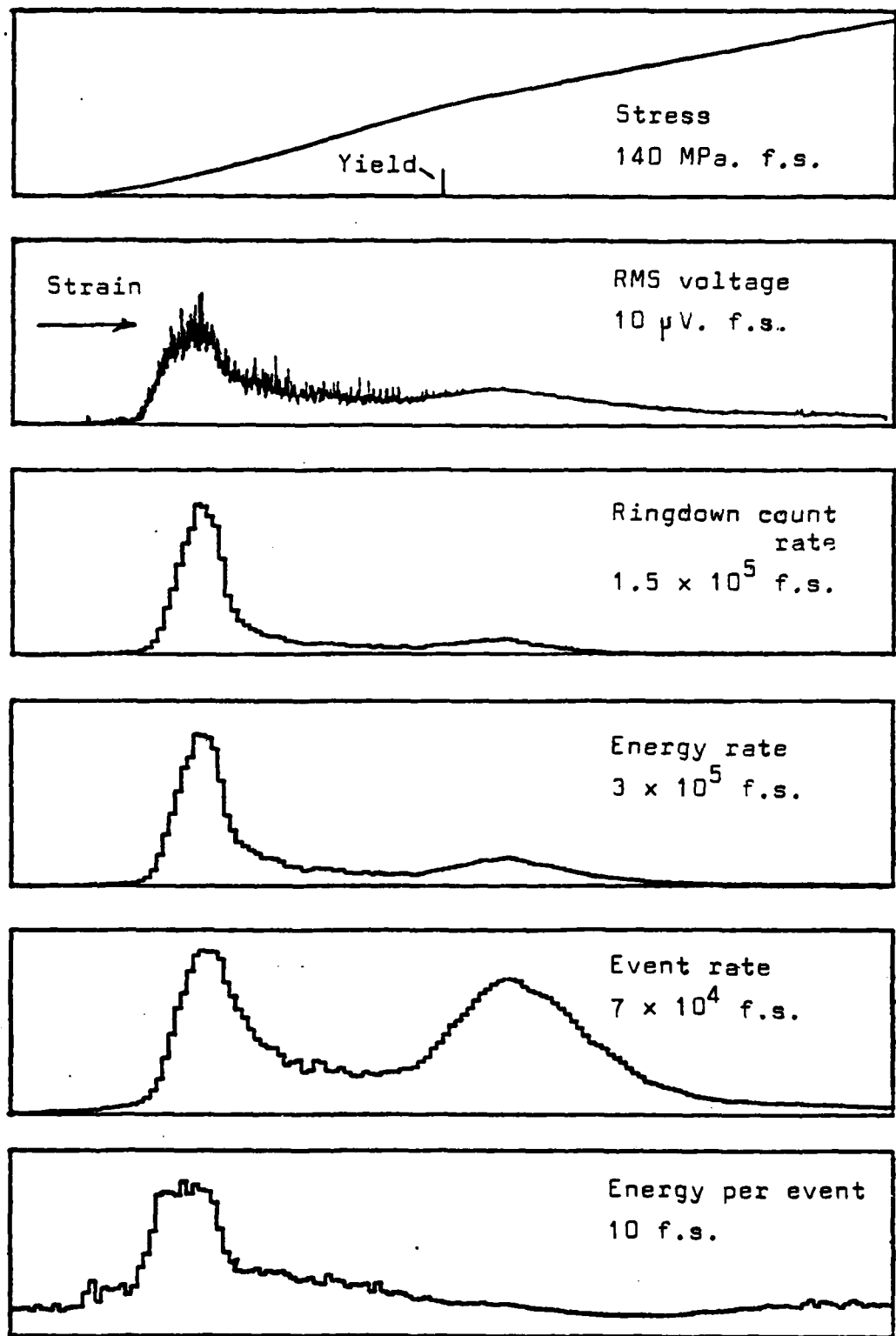


Figure 6. Various acoustic emission parameters and stress as a function of strain for a AZ31 B magnesium sample tested in tension. Sample axis is perpendicular to plane of plate.

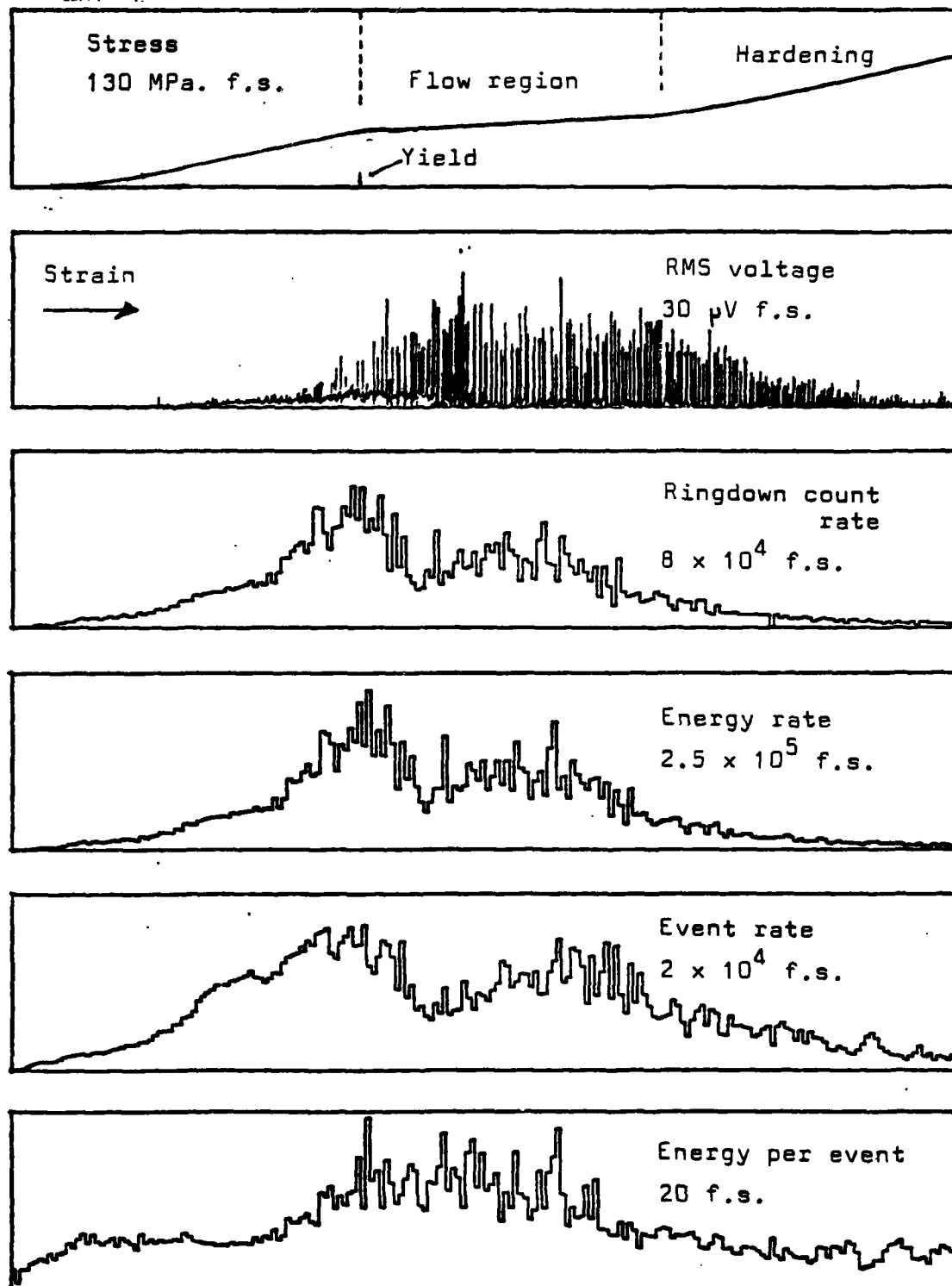
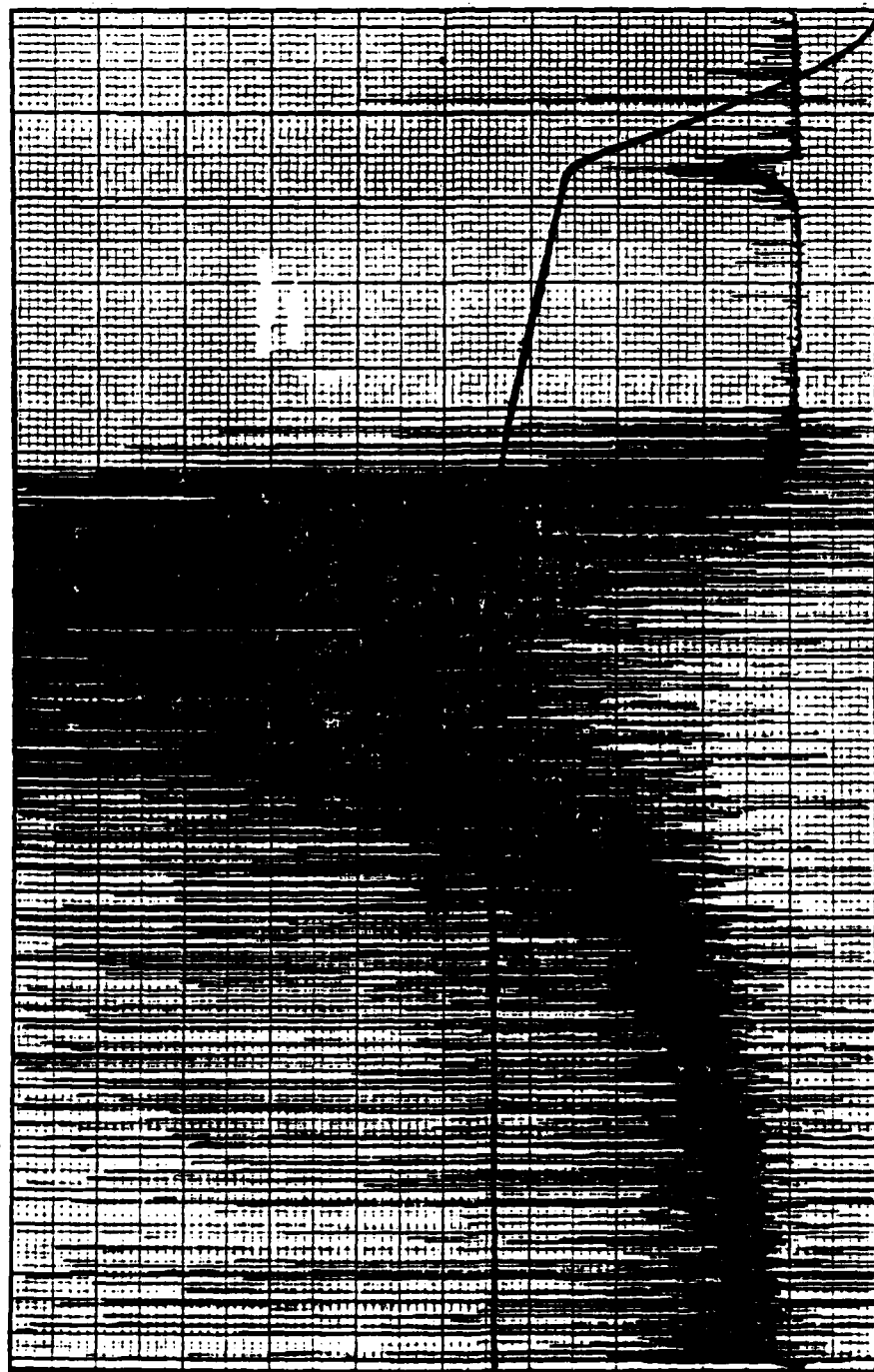


Figure 7. Various acoustic emission parameters and stress as a function of strain for a AZ31 B magnesium sample tested in tension. Sample axis is parallel to plane of plate.

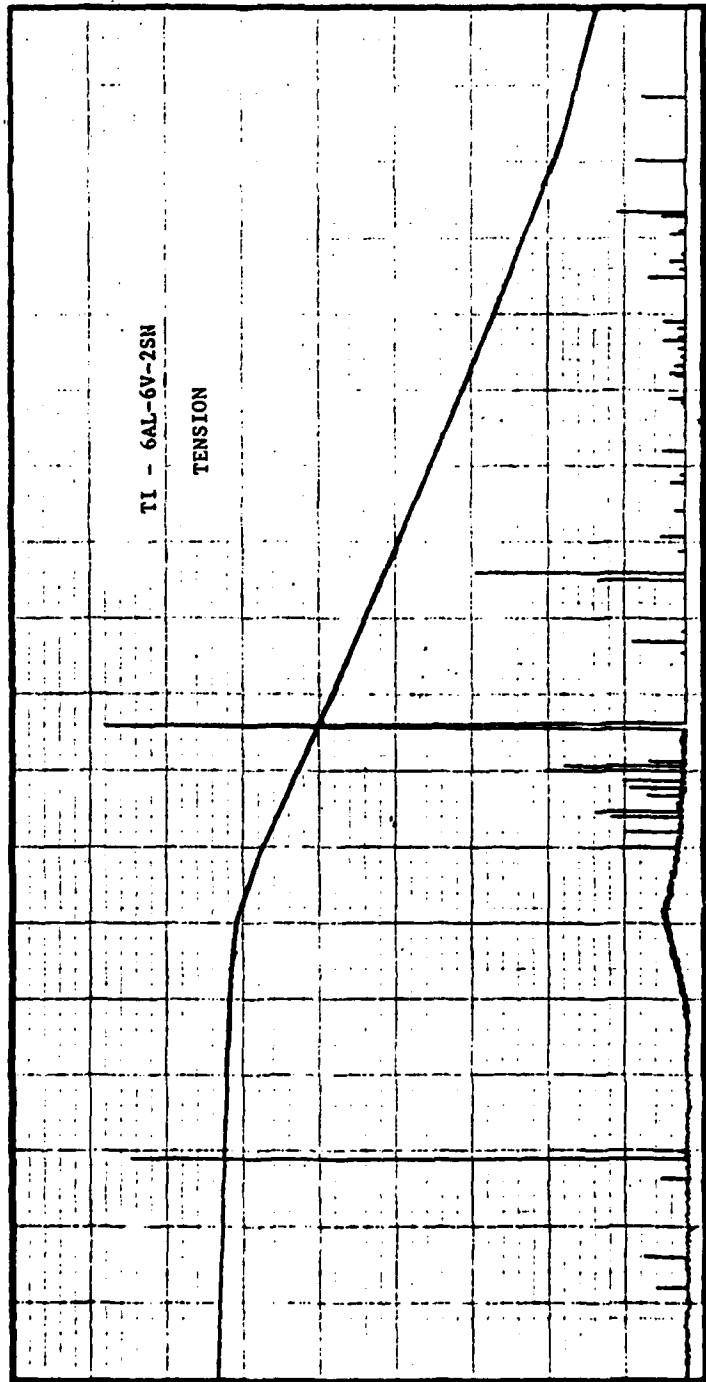
Acoustic emission rms voltage load



Deflection (constant crosshead velocity)

Figure 8. Acoustic emission measured by rms voltage and load as a function of deflection for a constant crosshead velocity tensile test. Sample material is pure titanium (50A).

Acoustic emission rms voltage load



Deflection (constant crosshead)

Figure 9. Acoustic emission measured by rms voltage and load as a function of deflection for a constant crosshead velocity tensile test. Sample material is Ti-6AL-6V-2SN alloy.

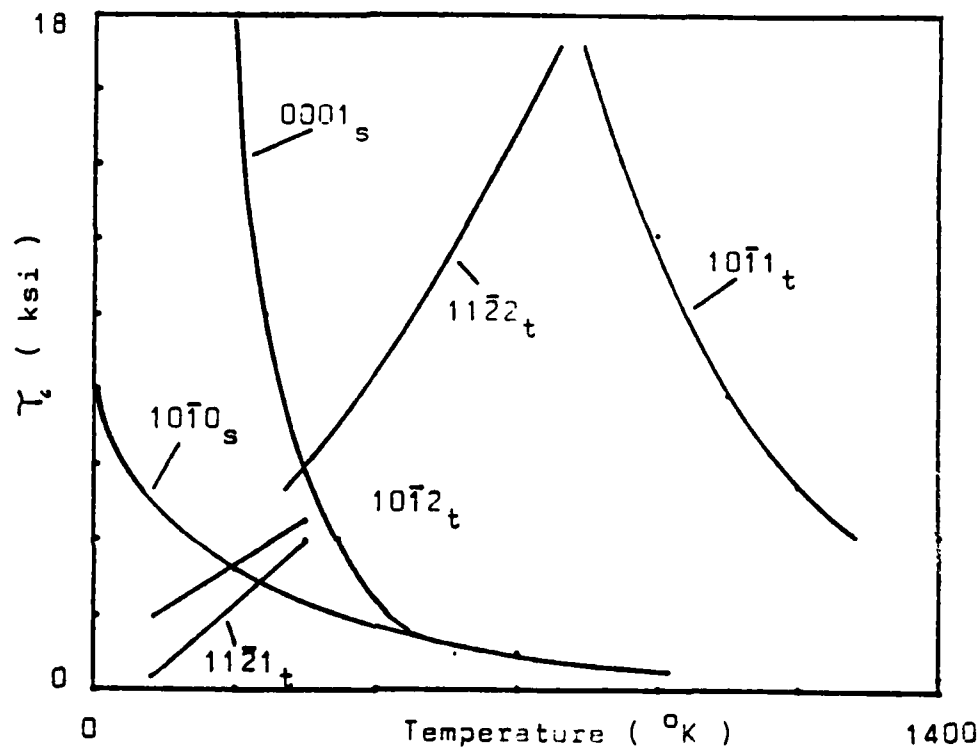


Figure 10. Temperature dependence of the critical resolved shear stress for various orientations of slip, and the activation stress for various twinning modes in titanium.

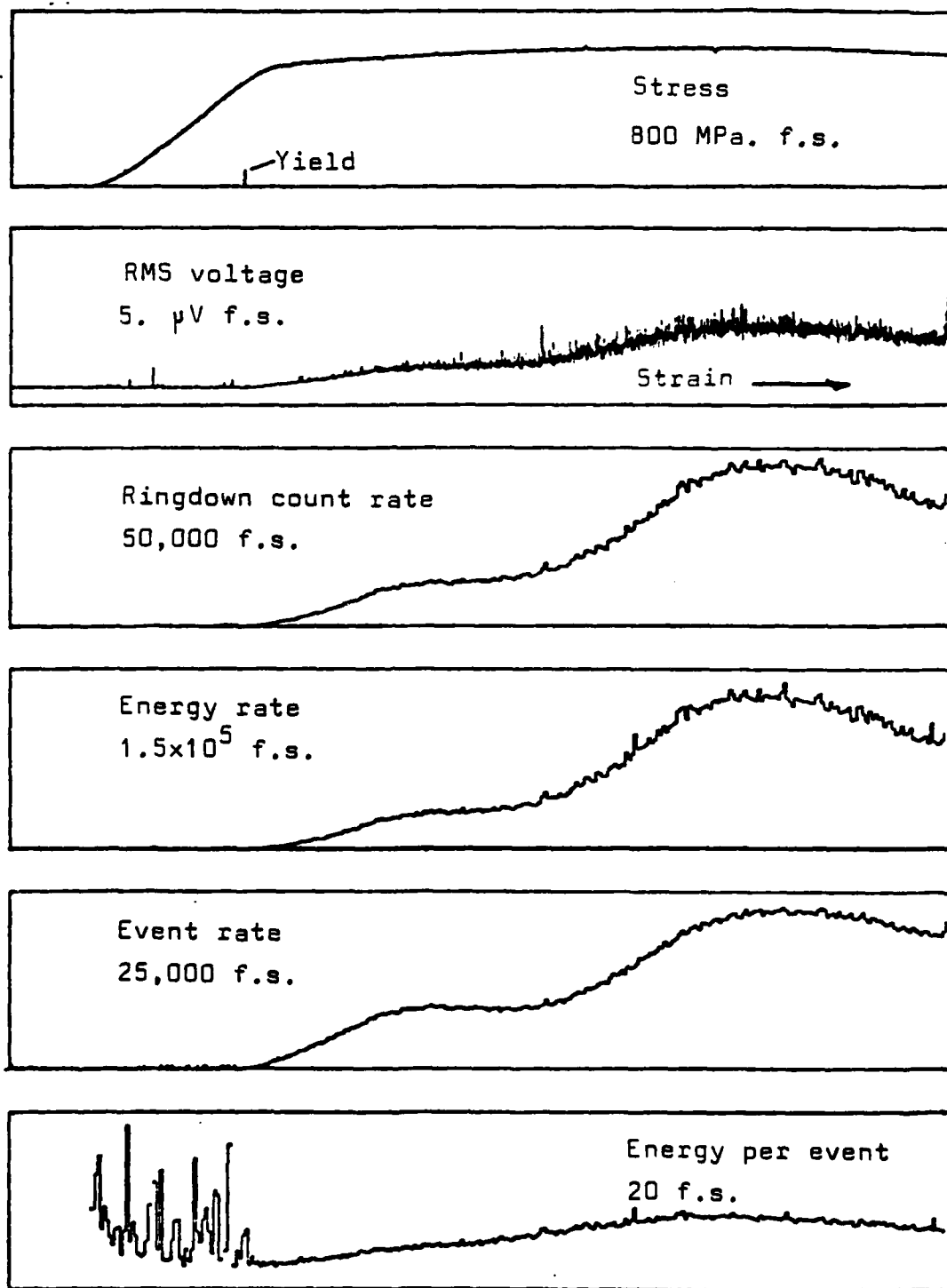


Figure 11. Various acoustic emission parameters and stress as a function of strain for a VP\* grade pure titanium tensile sample. All acoustic emission data except rms voltage given in counts per 5 sec.

\*VP is a trademark of Materials Research Corp.

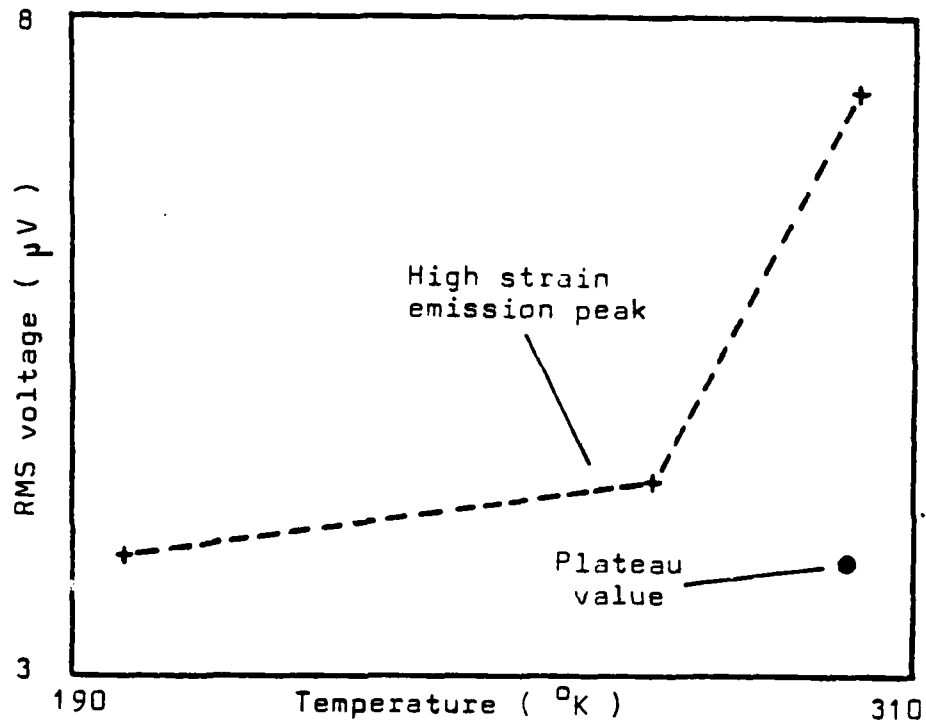


Figure 12. Acoustic emission measured by rms voltage at the high strain emission peak maximum as a function of test temperature. VP\* grade titanium tested in tension.

\*VP is a trademark of Materials Research Corp.

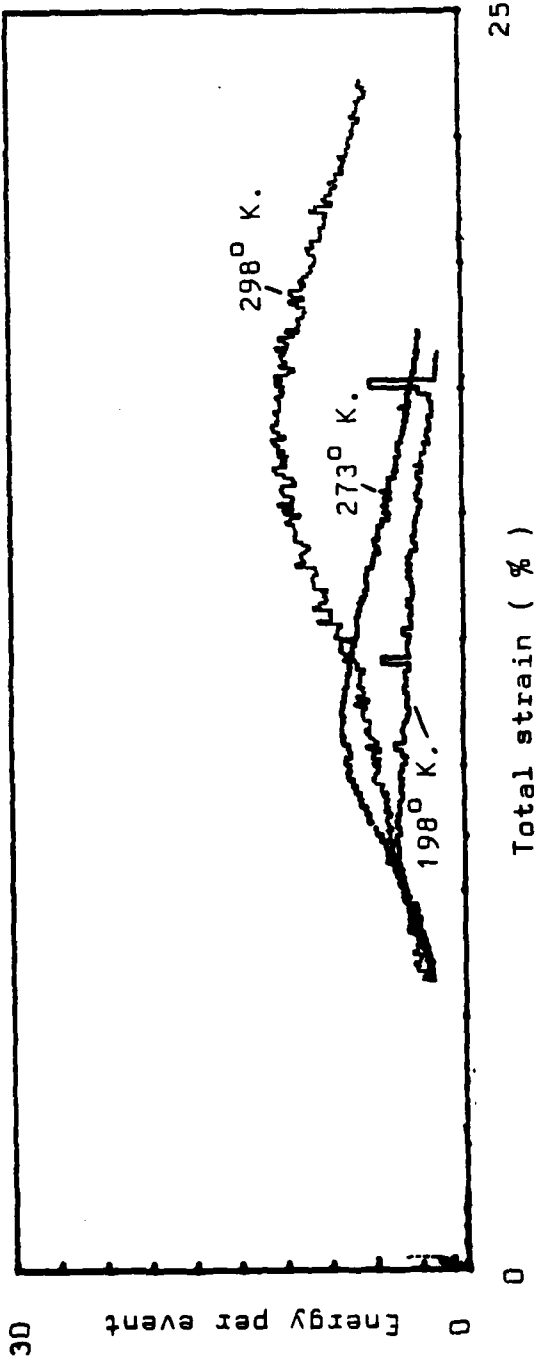


Figure 13. Acoustic emission energy per event for VP\* titanium tested in tension as a function of test temperature.

\*VP is a trademark of Materials Research Corp.

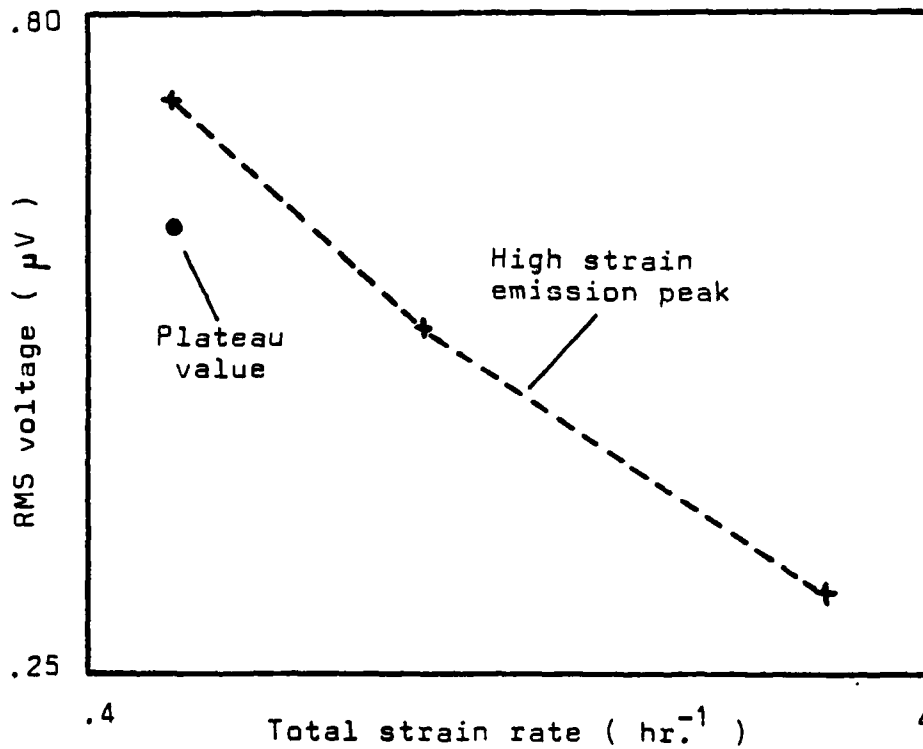


Figure 14. Acoustic emission measured by rms voltage at the high strain emission peak maximum as a function of total strain rate. VP\* grade titanium tested in tension.

\*VP is a trademark of Materials Research Corp.

CHANGES IN ACOUSTIC EMISSION PEAKS IN  
PRECIPITATION STRENGTHENED ALLOYS WITH HEAT TREATMENT

C.R. Heiple  
Rockwell International  
Rocky Flats Plant  
P.O. Box 464  
Golden, Colorado 80401

S.H. Carpenter  
Department of Physics  
University of Denver  
Denver, Colorado 80208

October, 1982

## ABSTRACT

Acoustic emission was measured during tensile deformation in a number of precipitation-strengthened alloys as a function of prior heat treatment. The alloys tested included 7075, 6061, and 2219 aluminum; a modified A-286 stainless steel (JBK-75) and an experimental beryllium--containing stainless steel; and Incoloy 903. A rms acoustic emission peak was observed in all the alloys near the onset of plastic flow, and a second peak was usually observed in 7075, 2219, and Incoloy 903 at plastic strains greater than one percent. Some evidence of a second peak was also observed in 6061 aluminum.

Changes with heat treatment in the stress and strain at which the second peak occurred were consistent with the peak arising from the fracture of inclusions. The shifts in the location of the peak were in a direction so as to make the stress on the inclusions at the second peak relatively insensitive to prior heat treatment. The acoustic emission signal amplitude distributions were also consistent with this interpretation. The strain at which the first acoustic emission peak occurred also varied with heat treatment, but the dependence of peak location on prior aging was different for the various alloys.

## INTRODUCTION

Acoustic emission has been measured during deformation as a function of prior heat treatment in a number of precipitation-strengthened alloys, including 7075, 6061, and 2219 aluminum alloys; JBK-75 (an alloy similar to A286) and KHB (an experimental alloy age-hardened with a NiBe precipitate) stainless steels; and Incoloy 903. The acoustic emission parameters measured included the rms acoustic emission as a function of strain, the peak height, plastic strain and stress at which any rms maxima occurred, and the amplitude distribution of the acoustic emission signals for various strain intervals.

The initial part of this investigation involved measuring, for a series of heat treatments, the height of the rms acoustic emission peak which occurs in these alloys near the onset of plastic flow. The results of these measurements have been reported elsewhere (Heiple, et. al., 1981). In addition to changes in peak height with prior heat treatment, the plastic strain at which the peak occurred also changed in a systematic way with heat treatment for some of the alloys tested. Beyond the rms acoustic emission peak near yield, a substantial second peak typically occurring after about 1 percent plastic strain was observed in three of the alloys - 7075 Al, 2219 Al, and Incoloy 903. Some indications of a second peak were also observed in 6061 Al. The location of this peak, as a function of heat treatment, and other characteristics of the second peak when it occurred are reported here. Amplitude distributions of the acoustic emission signals changed during the tests for some of these alloys. Amplitude distributions were taken for different positions on the acoustic emission peaks and at strains beyond the peaks.

## EXPERIMENTAL

Acoustic emission was detected during tensile tests with a Dunegan-Endevco (D/E) S140 transducer, which is a PZT-5A piezoelectric, longitudinally resonant-type transducer with a 140 kHz resonant frequency. The transducer was located on the gage section of the samples and was coupled to the sample with a viscous resin (Dow 276-V9). The output of the transducer was amplified with a Panametrics Model 5050AE-160A preamplifier (tests on Incoloy 903 used instead a D/E Model 802P preamplifier) and amplified further with a D/E Model 301 totalizer with a frequency bandpass of 100-300 kHz. Measurements were generally made with a system gain of 100 dB (85 dB for Incoloy 903). The amplified and bandpassed signal was measured with a Hewlett Packard 3400 A rms voltmeter. Amplitude distributions of the acoustic emission signals were determined after preamplification (60 dB gain) with a D/E 920 Distribution Module. Detailed measurements were made on 7075, 6061, and JBK-75, with less extensive measurements on the other alloys. Near the end of the study, a Nicolet Explorer III digital oscilloscope was obtained. Traces of the acoustic emission signal after preamplification were obtained at several strains for a few samples of 7075 Al and JBK-75.

Deformation of the tensile samples was produced with a universal testing machine, having a screw-driven crosshead, at a nominally constant crosshead speed of 0.05 mm/min. The load on the sample was obtained from the testing machine load cell. Sample deformation was measured with a 0.5 in., 10 percent extensometer attached to the tensile bar gage section. An extensometer was not used for the Incoloy 903 tests and sample deformation was calculated from the load-time curve, with testing machine deformation subtracted.

Outputs from the rms voltmeter, load cell, and extensometer were all recorded on strip chart recorders, yielding a record of all these parameters versus time. Stress and rms voltage were then replotted from these data versus strain. Noise was subtracted from the measured rms

acoustic emission voltage using the relation  $V_{rms}^2 = rms_m^2 - rms_n^2$ , where  $V_{rms}$  is the actual rms acoustic emission voltage,  $rms_m$  is the measured rms acoustic emission voltage, and  $rms_n$  is the rms noise voltage (Hamstad and Mukherjee, 1974).

The tensile bars used for most of the tests had a circular cross section of 4 mm diameter with a 19 mm reduced section and threaded ends. This tensile bar is one of the small-size round tension test specimens proportional to the standard round specimen (see Figure 8 of ASTM, 1979). Tension samples for testing KHB and Incoloy 903 were pin-loaded, sheet-type specimens which were essentially subsize versions of the standard pin-loaded tension test specimen (see Figure 7 of ASTM, 1979) and had a reduced section of about 25 mm. The grips of all samples were preloaded to at least 150 percent of the expected ultimate load before testing in order to minimize acoustic emission from the grips during the actual test.

With the exception of JBK-75 and KHB stainless steels, the alloys tested are commercial alloys whose aging behavior has been extensively investigated and described in the literature. The available information is summarized in Heiple, et. al., 1981. The compositions and heat treatments used for all the alloys tested are given in Tables 1-4. Because neither JBK-75 or KHB are commercial alloys, a brief description of them is included below.

Alloy JBK-75 is an age-hardenable austenitic stainless steel based on the commercial A286 alloy, but with chemistry modifications to improve resistance to hot cracking during welding (Brooks and Krenzer, 1974; Brooks, 1974). The primary modifications are an increase in nickel and a decrease in Mn, C, P, S, B, and Si. The composition range for JBK-75 is given in Table 3. Age hardening is achieved by precipitation of  $\gamma'$ ,  $M_3$  (Ti,Al), after solution heat treatment (Thompson and Brooks, 1975). The  $\gamma'$  precipitates as spherical coherent particles in the range 500-850°C. The  $\gamma'$  precipitates grow with increased aging time and

TABLE 1

## Nominal Composition of Commercial Aluminum Alloys Studied

	<u>2219</u>	<u>6061</u>	<u>7075</u>
Cr		0.2	0.23
Cu	6.3	0.28	1.6
Mg		1.0	2.5
Mn	0.3		
Si		0.6	
Zn			5.6
Zr	0.18		
V	0.1		
Ti	0.06		
Al	Balance	Balance	Balance

TABLE 2

## Heat Treatments Used for Commercial Aluminum Alloys

Alloy	Solution Treatment*	Ageing Treatment	Temper Designation	Predominant Precipitate Expected
2219	550°C, 1.5 hr	20°C, > 96 hr	T4	GP (1)
	550°C, 1.5 hr	20°C, > 96 hr; 190°C, 30 hr	T62	GP (2)
	550°C, 1.5 hr	20°C, > 96 hr; 250°C, 48 hr	Overaged	$\theta'$
	550°C, 1.5 hr	415°C, 1 hr; Cool $\leq$ 25°C/hr	0	$\theta$
6061	545°C, 15-20 min	-78°C, < 2 hr	-	None
	545°C, 15-20 min	20°C, - 6 months	-	GP needles
	545°C, 15-20 min	175°C, 1 hr	-	GP needles
	545°C, 15-20 min	175°C, 4 hr	-	Mg <sub>2</sub> Si Rods
	545°C, 15-20 min	175°C, 8 hr	T6	Mg <sub>2</sub> Si Rods
	545°C, 15-20 min	205°C, 24 hr	Overaged	Mg <sub>2</sub> Si platelets
7075	482°C, 15-20 min	-78°C, < 2 hr	-	None
	482°C, 15-20 min	120°C, 1 hr	-	GP spheres
	482°C, 15-20 min	120°C, 8 hr	-	GP spheres
	482°C, 15-20 min	120°C, 25 hr	T6	GP spheres
	482°C, 15-20 min	175°C, 8 hr	- T73	M' and/or M MgZn <sub>2</sub>

\* All samples water quenched after solution heat treatment.

TABLE 3

## Composition of Iron - Base Alloys Studied

	JBK-75	KHB, Heat 5	Incoloy 903
Cr	13.5 - 16	20	
Ni	29.0 - 31.0	30.5	37.5
Co		.05	15.3
Mo	1.0 - 1.5	.01	
Mn	0.30 max	.2	.15
C	0.01 - 0.03	.027 - .058	.03
P	0.010 max		
S	0.010 max		.004
Si	0.20 max	.3	.07
V	0.1 - 0.5		
Ti	2.0 - 2.3	.07	1.4
Al	0.15 - 0.35	.01	1.0
B	.001 max		
Be		.44	
Nb + Ta			2.8
Fe	Balance	Balance	Balance

TABLE 4

## Heat Treatments Used for Iron - Base Alloys

Alloy	Solution Treatment*	Ageing Treatment	Predominant Precipitate Expected
JBK-75	985°C, 1 hr He quench	Set 1**: None Set 1: 675°C; 1/2, 1,4,16,64 hr	None $\gamma'$
	985°C, 1 hr He quench	Set 2**: 720°C; 1/2, 1,2,4,16,64,256 hr	$\gamma'$ , $\eta$ at 16 or more hours
	985°C, 1 hr He quench	Set 3: None Set 3: 720°C; 1,4, 16,64,256 hr	None $\gamma'$ , $\eta$ at 16 or more hours
KHB	1150°C, 1 hr	500°C; 1/2,1,2,4,8, 16,32,72 hr	GP zones only
	1150°C, 1 hr	600°C; 1/2,1,2,4,8, 16,32,72 hr	GP zones initially, $\beta'$ after 1-4 hours
Incoloy 903	980°C, 1 hr	None	None
	980°C, 1 hr	720°C, 8 hr, cool at 100°C/hr to 620°C, hold 8 hr	$\gamma'$
	980°C, 1 hr	720°C, 16 hr	$\gamma'$

\* Except as noted, all samples water quenched after solution heat treatment and aging treatment.

\*\* Sets 1 and 2 homogenized 4 hr at 1205°C and cold swaged 62 percent prior to solution treatment.

provide increased strength. Overaging leads to conversion of the  $\gamma'$  into the equilibrium  $\eta$ ,  $\text{Ni}_3\text{Ti}$ , which usually forms a cellular precipitate and generally nucleates at grain boundaries. Formation of optically observable  $\eta$  begins well before maximum strength is achieved by aging. As would be expected from the complex composition of the alloy, a number of minor phases have been reported (Thompson and Brooks, 1975). The precipitates expected after the heat treatments used in this study are given in Table 4.

The KHB alloy is an experimental austenitic stainless steel which originated from an effort to make a useful alloy from beryllium-contaminated type 304L stainless steel scrap. Substantial nickel additions to 304L were required to maintain an austenitic structure because Be is a powerful ferrite stabilizer. The composition of experimental heat 5, which was used for the work reported here, is given in Table 3. The alloy is single phase austenite after solution heat treatment at  $1150^\circ\text{C}$  followed by a water quench. The initial precipitates during aging between  $500$  and  $600^\circ\text{C}$  are coherent disc-shaped Guinier-Preston (GP) zones. At  $600^\circ\text{C}$  and above, these GP zones grow into semicoherent disc-like  $\beta'$   $\text{NiBe}$ . Aging at higher temperatures will convert the  $\beta'$  into incoherent  $\beta$   $\text{NiBe}$  (Carr and Heiple, 1980).

## RESULTS

### A. Characteristics of the Second Acoustic Emission Peak

Acoustic emission and stress versus strain are plotted in Figure 1 for a 7075 aluminum sample. The two acoustic emission peaks are clearly distinguished for this material and heat treatment. Peak I refers to the peak near yield, and Peak II refers to the peak at higher strains. Note that in Figure 1 and all subsequent figures, acoustic emission signal voltages are referred to the transducer output, i.e., the measured or calculated values have been divided by amplifier gain.

The height of Peak II in 7075 Al is essentially independent of heat treatment, as shown in Figure 2. The response of Peak I to heat treatment is also shown in Figure 2 for comparison. The stress and plastic strain at which Peak II occurred in 7075 are shown in Figure 3. The same variables are plotted for 2219 Al in Figures 4 and 5, and for Incoloy 903 in Figures 6 and 7. Note that Peak II was not found in the severely overaged, "O", condition in 2219 Al or in the solution treated and quenched condition in Incoloy 903. Peak II, if it existed in 6061 Al, was too small and broad to be characterized. The height of Peak II appears to depend on heat treatment in both 2219 Al and Incoloy 903, although the number of available data points is quite small.

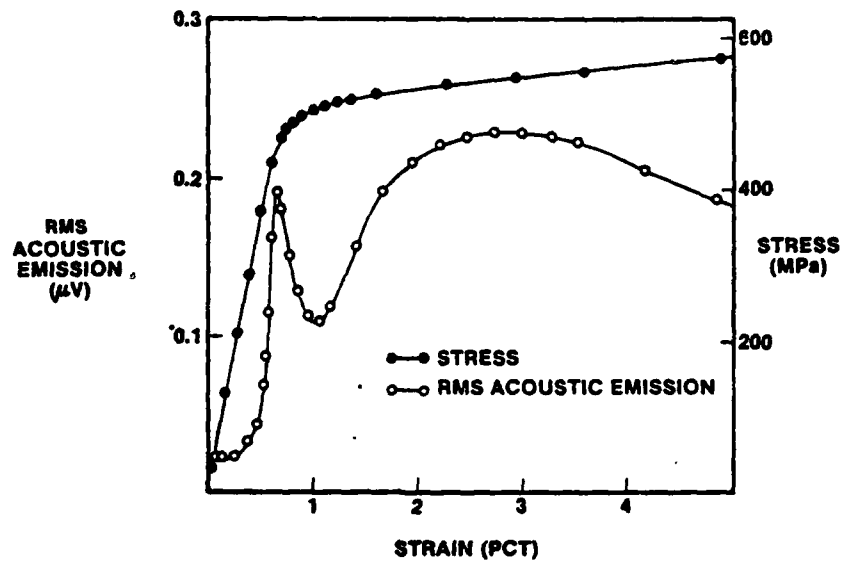


Figure 1. Acoustic emission (referred to the transducer output and corrected for noise) and stress for a 7075 Al tensile bar aged 1 hr at 120°C.

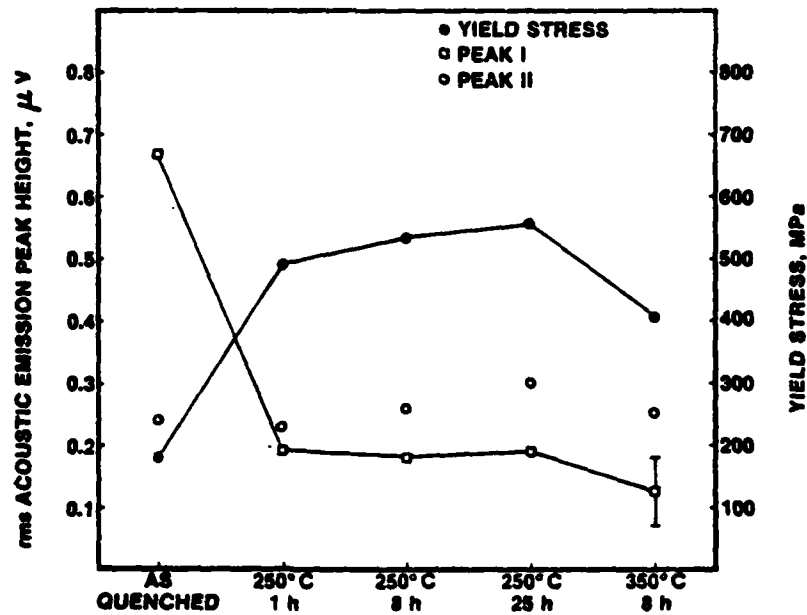


Figure 2. Height of Peaks I and II, and yield stress, in 7075 Al as a function of heat treatment.

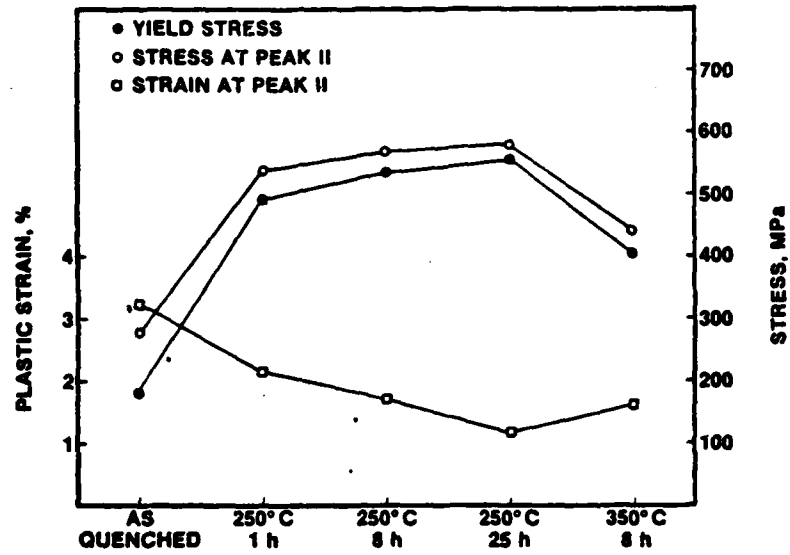


Figure 3. Stress and plastic strain at the Peak II maximum, and yield stress, in 7075 Al as a function of heat treatment.

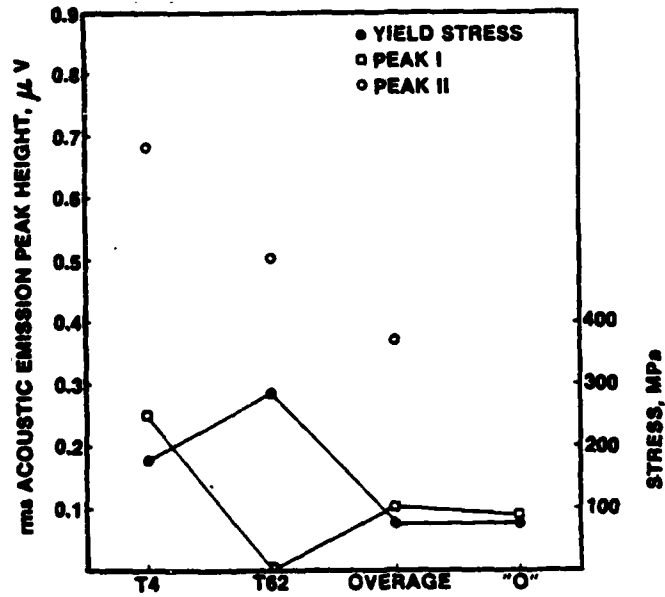


Figure 4. Height of Peaks I and II, and yield stress, in 2219 Al as a function of heat treatment.

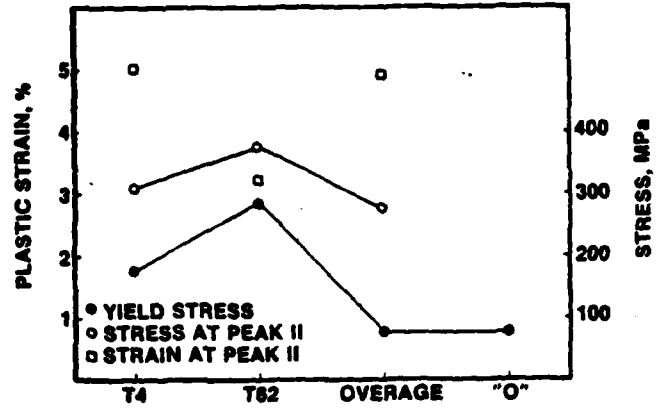


Figure 5. Stress and plastic strain at the Peak II maximum, and yield stress, in 2219 Al as a function of heat treatment.

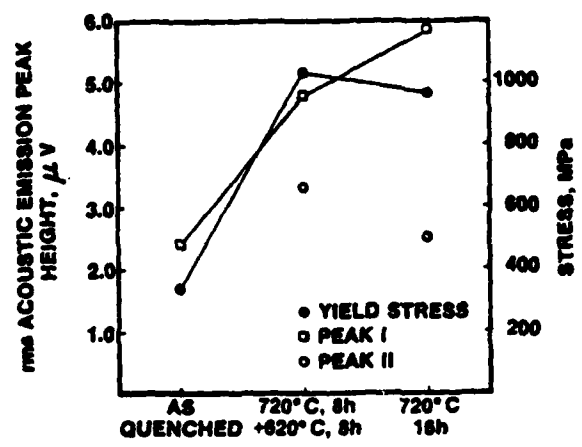


Figure 6. Height of Peaks I and II, and yield stress, in Incoloy 903 as a function of heat treatment.

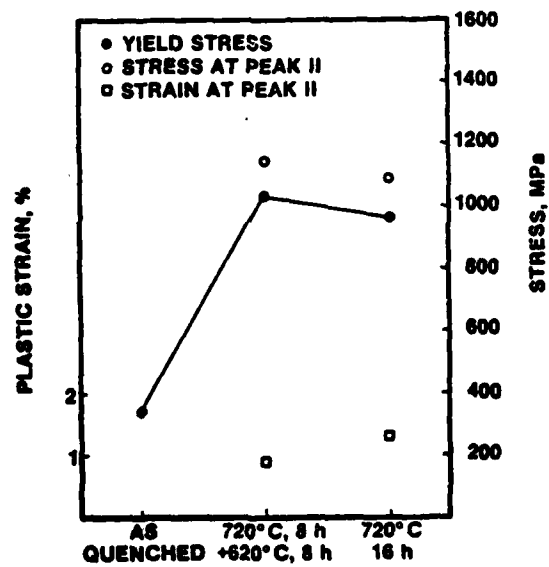


Figure 7. Stress and plastic strain at the Peak II maximum, and yield stress, in Incoloy 903 as a function of heat treatment.

## B. Plastic Strain at the Peak I Maximum

The first rms acoustic emission peak occurred at strains less than 0.2 percent, commonly used to define yield, for all materials tested after all heat treatments employed. The location of the peak varied systematically with heat treatment for several of the alloys, however, the dependence of peak location on aging varied for these alloys. In KHB, the plastic strain at which the peak occurred increased substantially with increasing aging time (and hence increasing yield strength) as shown in Figure 8. However, in JBK-75, the peak instead shifted to somewhat lower plastic strains with increased aging (Figure 9). The shift was fairly small and was not apparent for initial aging, well before maximum strength (Figure 10). In 6061, the plastic strain at which the peak occurred was largest in the slightly underaged condition, and decreased sharply for either more or less aging (Figure 11). The peak location appeared independent of aging in 7075 (Figure 12), and insufficient data were available to establish a trend in 2219 (Figure 13).

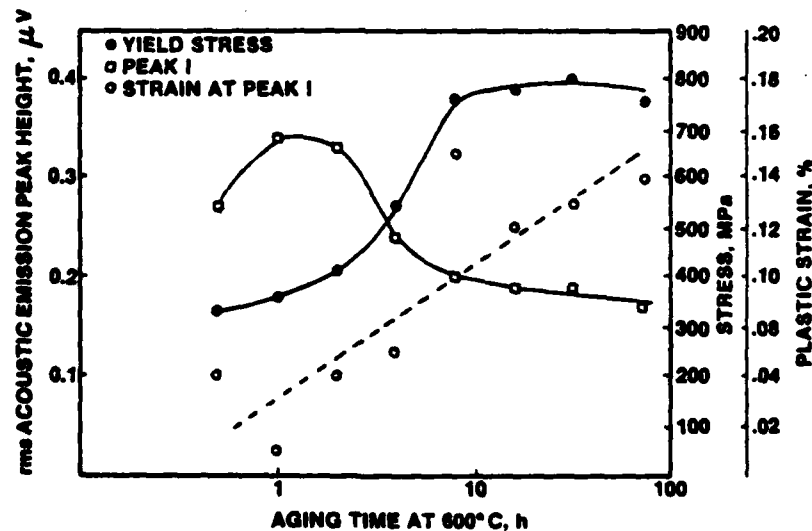


Figure 8. Plastic strain and rms acoustic emission at the Peak I maximum, and yield stress, in KHB stainless steel as a function of aging time.

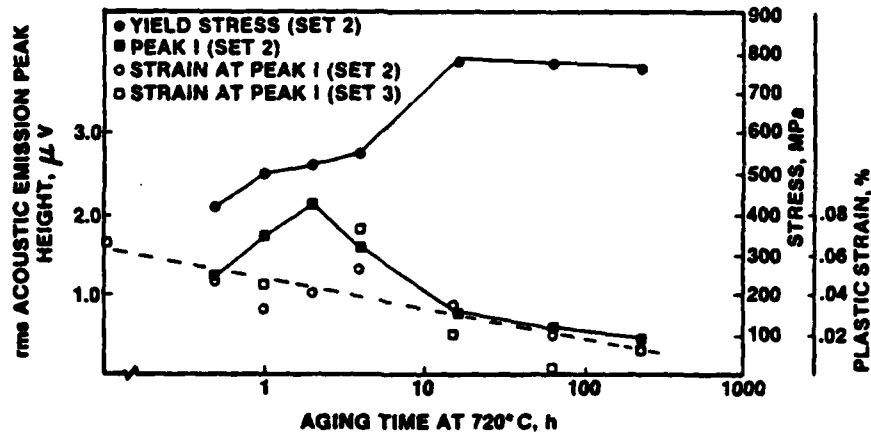


Figure 9. Plastic strain and rms acoustic emission at the Peak I maximum, and yield stress, in JBK-75 stainless steel as a function of aging time at 720 °C.

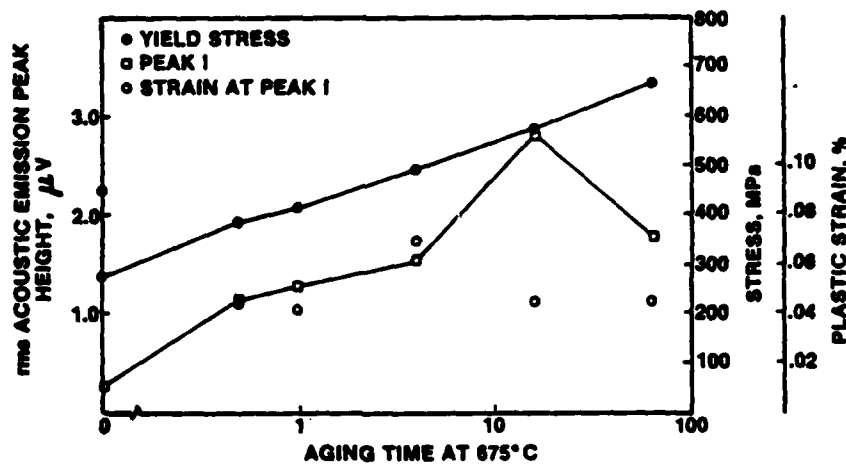


Figure 10. Plastic strain and rms acoustic emission at the Peak I maximum, and yield stress, in JBK-75 stainless steel as a function of aging time at 675 °C.

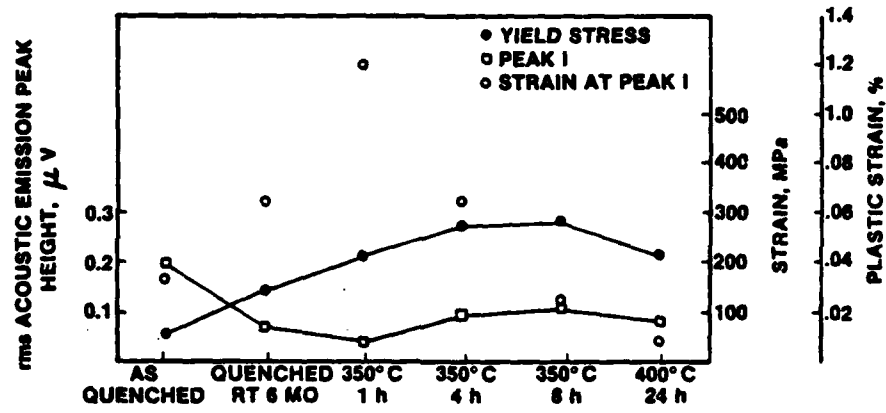


Figure 11. Plastic strain and rms acoustic emission at the Peak I maximum, and yield stress, in 6061 Al as a function of heat treatment.

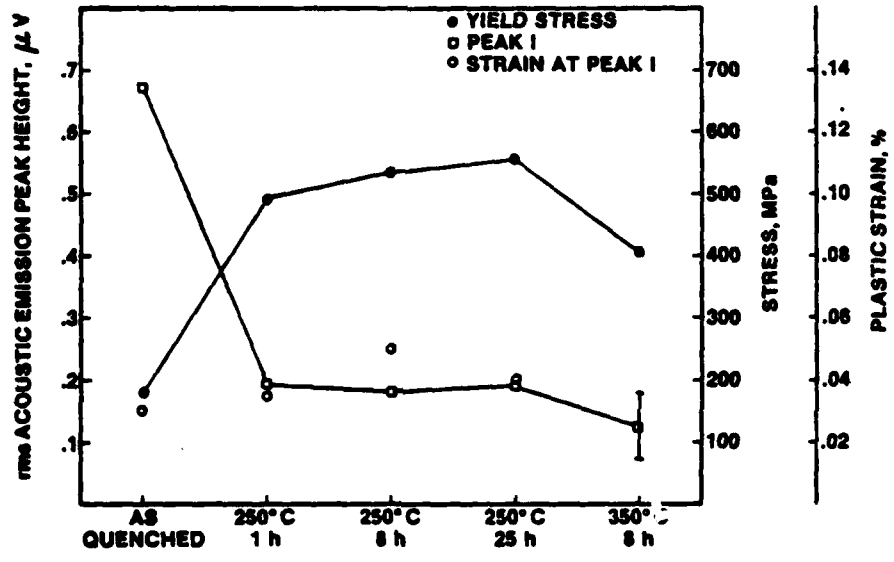


Figure 12. Plastic strain and rms acoustic emission at the Peak I maximum, and yield stress, in 7075 Al stainless steel as a function of aging time at 675°C.

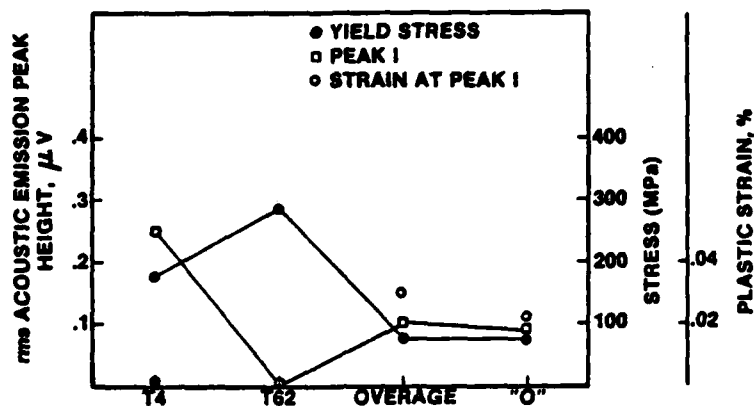


Figure 13. Plastic strain and rms acoustic emission at the Peak I maximum, and yield stress, in 2219 Al as a function of heat treatment.

### C. Amplitude Distributions

Amplitude distributions were taken at different points along the acoustic emission curves for all heat treatments attempted in 7075 Al. The amplitude distributions of signals in strain intervals including most of Peak I were independent of heat treatment, except there was a slightly larger proportion of higher amplitude events in the solution treated and quenched condition. The fraction of high amplitude events in Peak II was higher than in Peak I. The amplitude distributions from Peaks I and

II are compared for a sample aged 8 hours at 250°C in Figure 14. The rms versus strain for the sample is included in this and subsequent figures of the same type, with the strain ranges indicated over which the amplitude distributions were taken. All amplitude distributions have been normalized by dividing the number of events at each amplitude by the total number of events in the distribution. The amplitude distribution for Peak II in Figure 14 was typical of all the heat treatments except 1 hour at 250°C. For that underaged condition, the amplitude distribution in Peak II was more like that in Peak I. Amplitude distributions were taken both on the rising and falling portion of Peak II for several samples and there was no significant difference.

The acoustic emission signal from 7075 appears continuous when monitored on an oscilloscope. However, the actual signal contains many small bursts. A 2000  $\mu$ sec portion of the acoustic emission signal from 7075 recorded after preamplification (60dB) of the transducer output is shown in Figure 15. The recording was taken near the Peak I maximum for a sample solution treated and quenched. Similar records are not available for the other heat treatments, but would be expected to be similar.

The behavior of the amplitude distributions from 6061 Al was quite similar to that observed in 7075 Al. Again there was little dependence of the amplitude distributions from Peak I on heat treatment, except that the solution treated and quenched sample had a slightly higher proportion of high amplitude events. No distinct Peak II was observed in 6061 Al, but signals from the strain range where Peak II would be expected had a substantially higher fraction of high amplitude events than the signals from Peak I. The amplitude distributions from Peak I and a strain region beyond Peak I are compared for a sample aged 8 hours at 350°C in Figure 16. Again, in the underaged condition (1 hour at

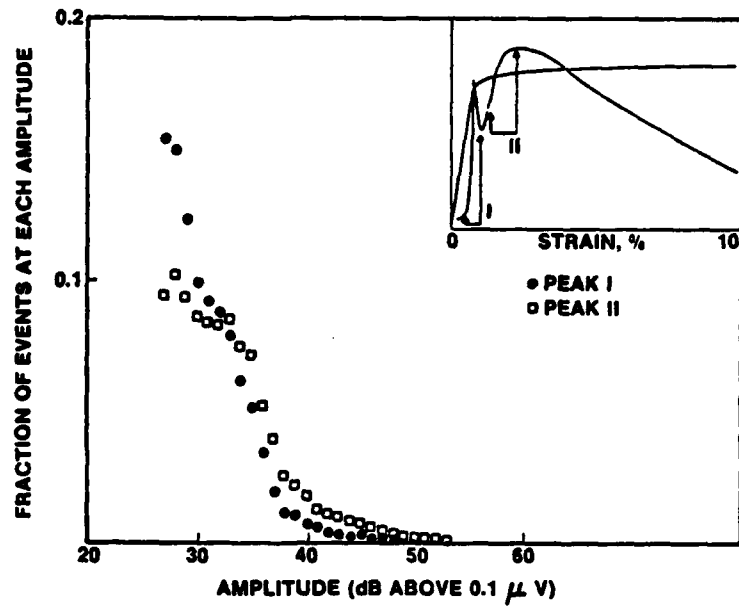


Figure 14. Comparison of amplitude distributions from Peaks I and II in 7075 Al aged 8 hr at 250 °C. The strain intervals over which the distributions were taken are indicated in the insert.

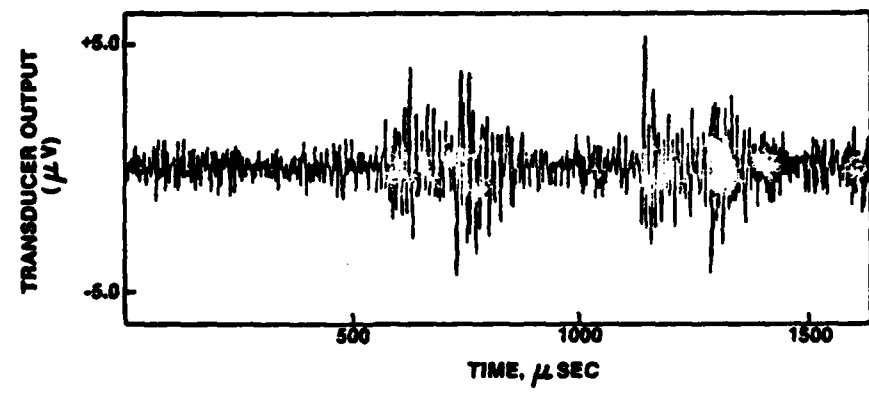


Figure 15. Acoustic emission signal near the Peak I maximum in 7075 Al in the solution treated and quenched condition.

350°C), the proportion of high amplitude signals was lower in the region where Peak II is expected than in samples more fully aged.

The most dramatic changes in amplitude distribution were observed in JBK-75. Only Peak I is observed in this alloy, and amplitude distributions were taken on the rising (low strain) side of the peak, the declining side, and well beyond the peak. A comparison of the amplitude distributions on the rising and falling sides of Peak I in a sample aged 4 hours at 675°C is given in Figure 17. The distributions well beyond the rms peak contained a somewhat smaller fraction of high amplitude events than the distributions on the declining side of the rms peak.

Portions of the acoustic emission signal from JBK-75 were recorded after preamplification. Both before and after the rms maximum, the signal consisted of fairly well defined bursts, Figure 18. However, at or near the rms maximum, the signal appeared like a classic continuous emission signal (Figure 19). Amplitude distributions close to the rms maximum could therefore not be obtained and would not be meaningful in any case.

There were modest changes in the amplitude distributions with heat treatment. The change was a shift of the amplitude distribution to higher amplitudes for heat treatments which increased the magnitude of the rms peak. This shift may be real, however, it could easily be an artifact associated with the increased level of "continuous" emission near the rms maximum.

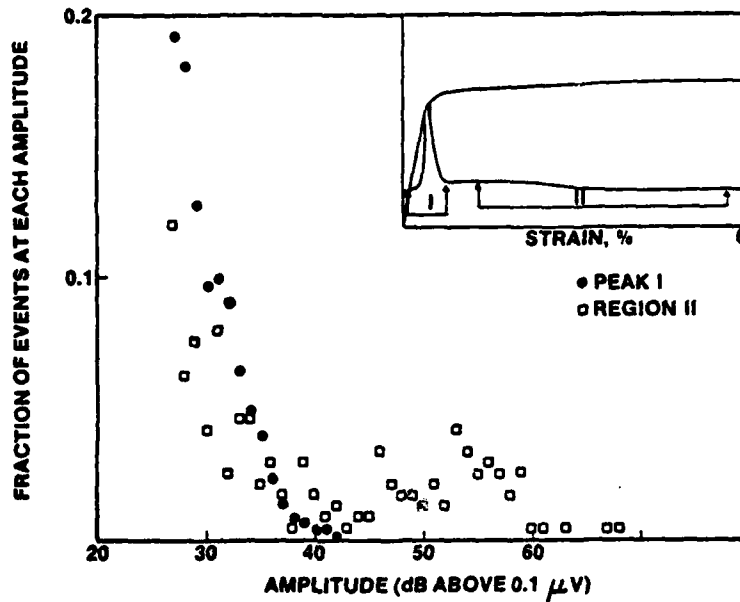


Figure 16. Comparison of amplitude distributions from Peak I and a region where Peak II is expected in 6061 aged 8 hr at 350°C. The strain intervals over which the distributions were taken are indicated in the insert.

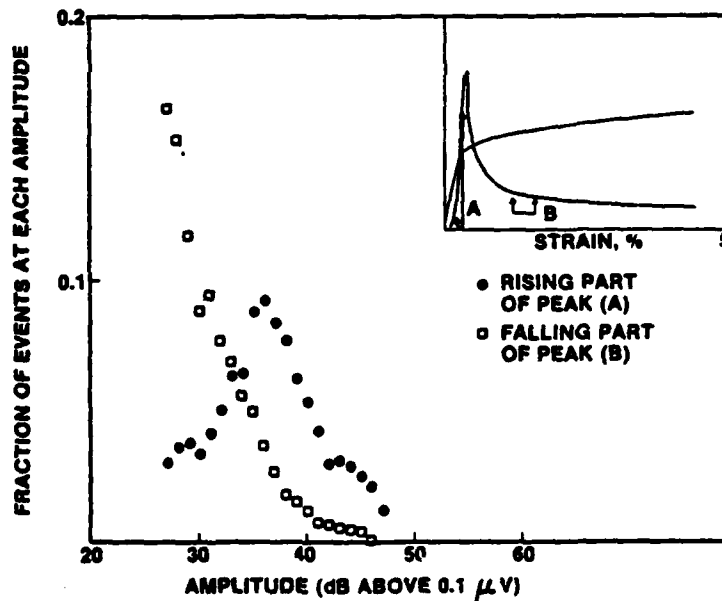
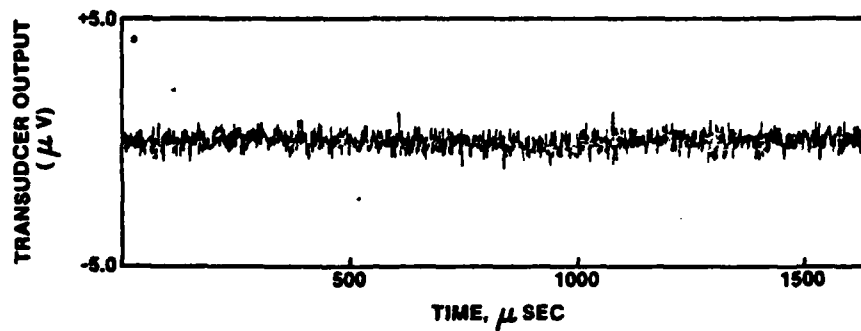
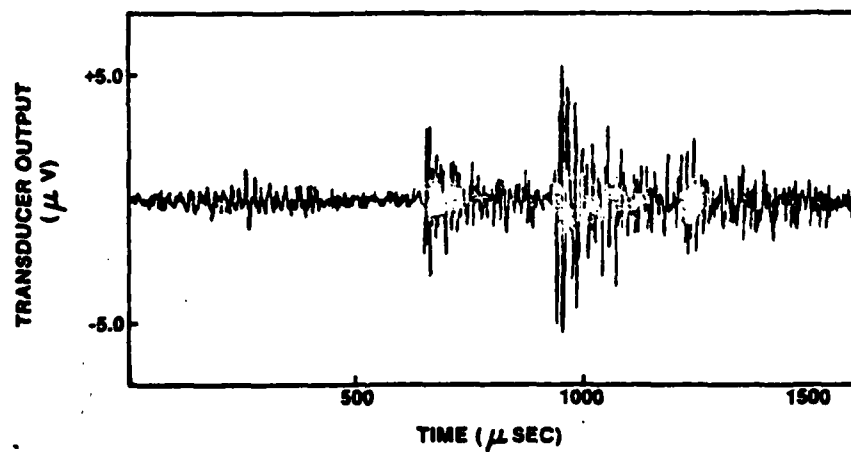


Figure 17. Comparison of amplitude distributions from the rising and falling portions of Peak I in JBK-75 aged 4 hr at 675°C. The strain intervals over which the distributions were taken are indicated in the insert.



(a)



(b)

Figure 18. Acoustic emission signal from JBK-75 aged 16 hr at 675°C. (a) system noise level (b) acoustic emission before the Peak I maximum.

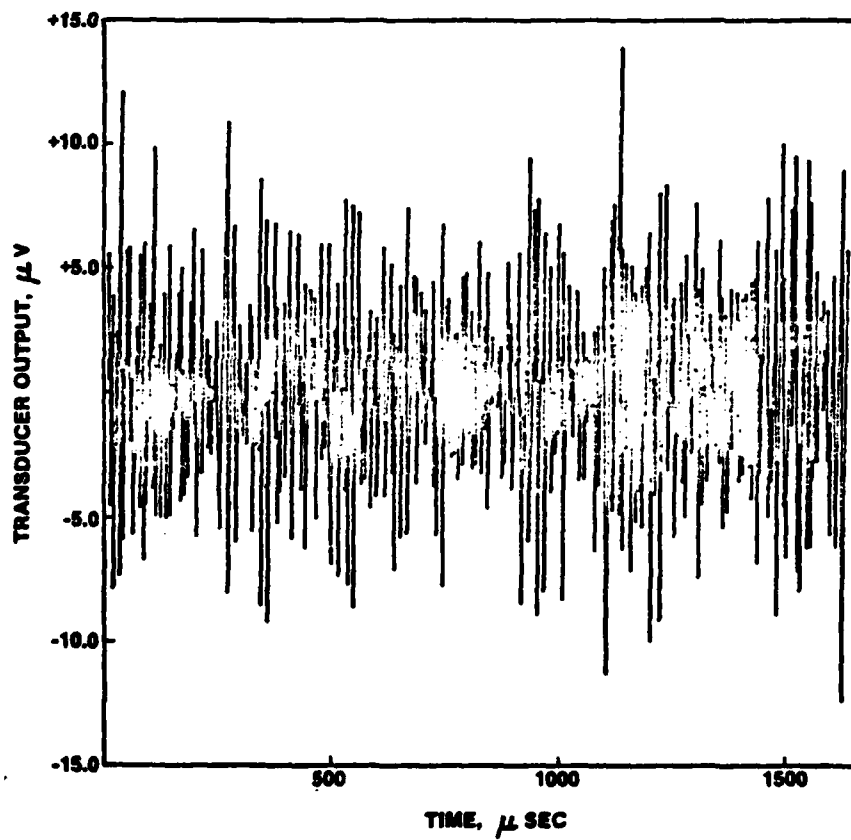


Figure 19. Acoustic emission signal at the Peak I maximum in JBK-75 aged 16 hr at 675°C.

## DISCUSSION

### A. Peak II

The acoustic emission in Peak II has been shown to arise in 7075 aluminum from the fracture and/or decohesion of inclusions (Carpenter and Higgins, 1977; Hamstad and Mukherjee, 1975; Cousland and Scala, 1981). Evidence supporting this conclusion includes the observations that Peak II essentially disappears in compression, that no internal friction peak is associated with Peak II while there is an internal friction peak concurrent with Peak I, and that Peak II only occurs after significant plastic strain.

McBride, et al., 1981, have recently investigated acoustic emission during slow crack growth in 7075 Al. They found quantitative agreement between the amplitude distribution of the burst acoustic emissions and the area size distribution of the large intermetallic inclusions in the alloy. When high purity material without these inclusions was tested, no burst emission was observed. Furthermore, when the alloy was in the "0" condition, no burst emission was observed either. In the latter case, inclusions on the fracture face were unbroken. These observations indicate the emission is associated with inclusion fracture rather than debonding.

Our observations on the behavior of Peak II with heat treatment are consistent with the peak arising from inclusion fracture during deformation. For the three alloys in which Peak II was definitely observed, the plastic strain at the Peak II maximum was lowest for the maximum-strength aging condition. (The stress at which the Peak II maximum occurred was correspondingly closest to the yield stress for the maximum-strength aging condition.) The data are consistent with the view that a substantial local stress, greater than the yield stress even in the maximum-strength aging condition, is required to fracture the inclusions in these alloys. The required local stress is achieved by a combination of the average applied stress and the stress concentration

resulting from plastic flow. Thus, less plastic flow is required to achieve particle fracture in the maximum-strength condition, as observed. If the matrix is sufficiently soft, then a stress high enough to cause general particle failure cannot be achieved and no Peak II occurs. This was apparently the case for the as-quenched condition in Incoloy 903 and the "0" condition in 2219 Al. Even though the yield strengths of the overaged and "0" condition 2219 Al were nearly the same, the ultimate tensile strength in the "0" condition was only 94 MPa while the overaged alloy work hardened much more and the stress at Peak II exceeded 270 MPa in the overaged condition.

During deformation, the stress on an inclusion differs from the stress in the matrix because of a difference in elastic moduli between matrix and inclusion (inhomogeneity stress), because of accommodation stresses between the inclusion which is assumed to only deform elastically and the plastically deforming matrix (plasticity stress), and because of different thermal expansion coefficients of inclusion and matrix (misfit stress) (Shibata and Ono, 1978a; 1978b).

The misfit stress does not, of course, arise from deformation but is generated during the heat treatment of the alloy. The calculated misfit stress for modest temperature changes can greatly exceed the matrix yield stress (Coade, et al., 1981). Under these conditions, plastic flow will instead occur in the matrix around the inclusions and the actual stress in the inclusions will be on the order of the matrix yield stress (Coade, et al., 1981).

Shibata and Ono (1978a) have calculated the inhomogeneity and plasticity stresses in an oblate spheroidal inclusion oriented so that the broad faces are parallel to the stress (and deformation) axis. The tensile stresses, inside the inclusions, parallel to the applied stress are given by

$$\sigma_{inh}^I = b \sigma_A \quad (\text{inhomogeneity stress}) \quad (1)$$

$$\sigma_p^I = C E^* \epsilon_p \quad (\text{plasticity stress}) \quad (2)$$

where  $\sigma_A$  is the applied matrix stress,  $E^*$  is Young's modulus of the inclusion,  $\epsilon_p$  is the matrix plastic strain, and  $b$  and  $c$  depend on the aspect ratio of the inclusion, the ratio of matrix and inclusion elastic moduli, and Poisson's ratios of the matrix and inclusion. The parameters  $b$  and  $c$  can be obtained from plots in the paper by Shibata and Ono (1978a) for the case when Poisson's ratio of the matrix and inclusion are both equal to 1/3.

Coade, et al., (1981) has measured experimentally the stresses on spherical silicon particles in an Al-Si-Mg alloy during deformation of up to 1 percent plastic strain. Their results agree with the prediction of Shibata and Ono (1978a) for the inhomogeneity stress, but not for the plasticity stress. Coade, et al., (1981) found instead that the plasticity stress was considerably smaller in magnitude and proportional to  $\epsilon_p^2$  at small strains, with possibly a linear dependence on  $\epsilon_p$  at higher strains.

A rough calculation of the stress on the inclusions at the Peak II maximum for various heat treatments of 7075 Al can be made on the basis of the work of Shibata and Ono (1978a,b) and Coade, et al., 1981. The inclusions in commercial 7075 Al are complex intermetallics with either Si or Fe as the major constituent and probably containing substantial oxygen (ElSoudani, 1973). To the best of our knowledge, Young's moduli of these inclusions have not been determined, but they probably lie in the range of a borosilicate glass (50-70 GPa; Anon, 1967),  $Cu_3Al$  (81 GPa; Guillet and LeRoux, 1967),  $Al_2Cu$  (95 GPa, Guillet and LeRoux, 1967), and FeO (145 GPa - calculated from a shear modulus of 54 GPa [Jackson, et al., 1978] assuming Poisson's ratio to be equal to 1/3). If

the inclusions are assumed plate-like (aspect ratio between 0.1 and 0.01) and  $E^*$  is taken to be 100 GPa ( $15 \times 10^6$  psi), then the constant  $b$  from Shibata and Ono (1978a) has a value of about 1.5. Using equation (1), the inhomogeneity stress calculated at matrix stresses corresponding to Peak II for the various heat treatments tested in 7075 Al is tabulated in Table 5.

Table 5

Estimated Stress (MPa) on Inclusions at Peak II Maximum, 7075 Al

<u>Heat Treatment</u>	<u>Yield Stress</u>	<u>Peak II Stress</u>	<u><math>\epsilon_p</math> Peak II (%)</u>	<u>Misfit Stress</u>	<u>Inhomogeneity Stress</u>	<u>Plasticity Stress</u>	<u>Total Stress</u>
Solution treated, Quenched	180	275	3.2	-180	410	470	700
1 hr 250°C	490	545	2.2	-490	820	310	640
8 hr 250°C	535	570	1.7	-535	855	230	550
25 hr 250°C	555	580	1.2	-555	870	150	465
8 hr 350°C	405	445	1.6	-405	670	220	485

If it is assumed that the plasticity stress is proportional to  $\epsilon_p^2$  as observed by Coade, et al., (1981) up to 0.5 percent plastic strain and is linear with  $\epsilon_p$  thereafter (with the slope at 0.5 percent plastic strain) and furthermore that the proportionality constant ( $1.6 \times 10^6$  MPa) is the same in 7075 Al as that found for spherical silicon particles in Al-Si-Mg alloy, then the plasticity stress can be estimated. The estimated plasticity stresses at the matrix strains corresponding to Peak II are tabulated in Table 5.

Finally, the misfit stress needs to be determined in order to estimate the total stress on the inclusions at Peak II for the various heat treatments. The coefficients of thermal expansion for the inclusions in 7075 Al are unknown, but probably lie between a borosilicate glass ( $4 \times 10^{-6}/^\circ\text{C}$  Anon, 1967) and refractory oxides ( $7-13 \times 10^{-6}/^\circ\text{C}$  Anon, 1967), considerably less than the value for aluminum ( $23 \times 10^{-6}/^\circ\text{C}$ )

(Anon, 1967). Taking the thermal expansion coefficient of the inclusions to be  $8 \times 10^{-6}/^{\circ}\text{C}$ , then the analysis of Shibata and Ono (1978b) predicts the maximum misfit stress to be -520 MPa upon cooling from 250°C to room temperature. (The aspect ratio of the inclusions was assumed to lie between 0.1 and 0.01, and  $E^*$  to equal 100 GPa, as above.) Thus, in agreement with Coade et al., (1981) it is reasonable to take the misfit stress to be equal to the yield stress.

The total estimated stress on the inclusions at the Peak II maximum is roughly the same for all heat treatments, as expected if the acoustic emission peak arises from inclusion fracture. The observations that the height of Peak II was independent of heat treatment and that no large shifts occurred with heat treatment in the acoustic emission signal amplitude distributions are also consistent with the inclusion fracture strength being insensitive to aging treatment.

The other observation on Peak II was that the amplitude distribution contained a higher fraction of high amplitude events than Peak I. This difference is consistent with the two peaks arising from different mechanisms. Finally, while no distinct second peak is observed in 6061 Al, the amplitude distribution of signals in the strain region where Peak II would be expected also contained more high amplitude events. Apparently there were not enough inclusions fracturing to create a distinct rms peak. Amplitude distributions with higher fractions of high amplitude events were not seen beyond Peak I in JBK-75 or KHB.

## B. Peak I

The major observation from Peak I, aside from changes in peak height with heat treatment, was the strong reduction in the size of the events with increasing strains from the rising to the falling sides of the peak in JBK-75. Peak I is generally accepted to arise from dislocation motion, although the details of the responsible dislocation mechanism are still the subject of some debate (Carpenter and Heiple, 1979). Most explanations for the reduction in emission with increasing strain following the rise to the peak invoke a reduction in dislocation glide distance with increasing strain caused by obstacles to dislocation motion created by the deformation itself. The shorter glide distance means the moving dislocations generate smaller elastic waves, and eventually the events become too small to be detected. At least in JBK-75, the predicted shift toward smaller events with increasing strain through Peak I is observed. Unfortunately, systematic amplitude distribution measurements were not taken on both sides of Peak I for the other alloys tested.

The varying dependencies on heat treatment of the location of Peak I in the alloys tested cannot be simply interpreted. The authors (Heiple, et al., 1981) have proposed that in alloy systems where cross slip is difficult, precipitates--if they are not too strong--can serve as breakable or cuttable pins and lead to the formation of dislocation avalanches, and thereby increase acoustic emission near the onset of plastic flow. In easy cross slip systems, dislocations tend to cross slip around precipitates, rather than form pile-ups, so that precipitates do not generally lead to increased acoustic emission except, perhaps, for a rather narrow size and strength range. These considerations do not apply if the pins are Cottrell atmospheres, and high levels of acoustic emission may be observed in either easy or difficult cross slip systems when solute atmospheres provide the pinning. The changes in the height of Peak I with heat treatment for the alloys described here are consistent with this interpretation.

Another model has also been proposed (Scruby, et al., 1981) based on increased glide distance of the dislocation packets associated with strain localization caused by cuttable precipitates. For both these models, the strain at which the maximum acoustic emission occurs depends on the details of the interaction between precipitates and dislocations. This interaction will be a function of the precise nature of the hardening precipitates, which differ for the different alloys. Different dependencies of peak location on heat treatment are therefore anticipated for the various alloys, but knowledge of the dislocation-precipitate interactions is presently inadequate to predict or even rationalize the observed changes in peak location.

## CONCLUSIONS

The magnitude, location in stress and strain, and amplitude distribution of the second acoustic emission peak, centered beyond 1 percent plastic strain, has been measured as a function of heat treatment in 7075 Al, 2219 Al, and Incoloy 903. The results are consistent with the peak arising from fracture of inclusions during deformation. Amplitude distributions suggest the same process occurred in 6061 Al, but there were insufficient inclusions fractured to produce a well defined acoustic emission peak. The fracture strength of the inclusions is insensitive to aging treatment, so the peak occurs at greater plastic strains in the underaged and overaged conditions. The increased plastic strains are required to build up sufficient stress for fracture in the inclusions. If the matrix is sufficiently soft, adequate stress to fracture the precipitates is not achieved and no peak occurs.

The first acoustic emission peak, centered near the onset of plastic flow, also shifted location in strain with aging treatment. The dependence on heat treatment was different for the various alloys, probably because of differences in the details of dislocation-precipitate interactions in the alloys.

In JBK-75, amplitude distributions on the declining (high strain) side of the first peak (and beyond) contained a much higher proportion of small amplitude events than distributions on the rising side of the peak. The shift in amplitude distribution is consistent with dislocation models for the origin of the acoustic emission peak near yield, which propose that the reduction in emission at larger strains arises from restriction of dislocation glide distances from obstacles created during plastic deformation.

## ACKNOWLEDGMENTS

Portions of this work were supported by the United States Department of Energy, Albuquerque Operations Office; by the National Science Foundation, Division of Materials Research, Grant No. DMR-1805112; and by the Air Force Office of Scientific Research, Division of Electronic and Solid State Sciences, Grant No. 77-3395. Their support is gratefully acknowledged.

C. B. Scruby, H. N. G. Wadley, K. Rusbridge, and D. Stockham-Jones  
(1981) *Met. Sci.* 15, 599-608.

M. Shibata and K. Ono (1978a) *Mater. Sci. & Eng.* 34, 131-137.

M. Shibata and K. Ono (1978b) *Acta Metall.* 26, 921-932.

A. W. Thompson and J. A. Brooks (1975) *Met. Trans. A*, 6A, 1431-1442.

Reprinted from

**Metal  
Science**

# Acoustic emission from dislocation motion in precipitation-strengthened alloys\*

C. R. Heiple, S. H. Carpenter, and M. J. Carr

A model is proposed to explain the effect of precipitation on acoustic emission from dislocation motion in age-hardening systems. The model is based on the hypothesis that a substantial number of dislocations must move rapidly and nearly simultaneously within a small volume of material in order to create detectable acoustic emission. In alloy systems where cross slip is difficult, precipitates, if they are not too strong, can serve as breakable pins and lead to the formation of dislocation avalanches and thereby increase acoustic emission near the onset of plastic flow. In easy cross slip systems, dislocations tend to cross slip around precipitates rather than form pile-ups, so the precipitates do not lead to increased acoustic emission. These considerations do not apply if the pins are Cottrell atmospheres, and high levels of acoustic emission may be observed in either easy or difficult cross slip systems when solute atmospheres provide the pinning. Acoustic emission measurements have been made as a function of heat treatment in several age-hardening systems with various stacking fault energies, elastic moduli, and precipitate strengths. For easy cross slip systems, including 7075 aluminium, 6061 aluminium, 2219 aluminium, and sterling silver, the acoustic emission was greatest in the solution-treated condition and was lowered by precipitation. For more difficult cross slip systems, including JBK-75, Incoloy 903, and an experimental beryllium-hardened austenitic stainless steel, the acoustic emission increased with increased aging times, for relatively short aging times, and then declined for longer aging times. No acoustic emission peak was observed in 17-10P, a stainless steel hardened by  $M_{23}C_6$  carbides. A relatively high acoustic emission peak was observed in 5083-0 and also in solution-treated 7075 and 6061, where serrated yielding indicated pinning by solute atmospheres.

MS/0756

© 1981 The Metals Society. C. R. Heiple and M. J. Carr are with Rockwell International, Energy Systems Group, Golden, Col., and S. H. Carpenter is in the Physics Department, Denver University, Denver, Col., USA.

Acoustic emission is a transient elastic wave generated by the rapid release of energy within a material. A wide variety of mechanisms has been proposed as capable of releasing enough energy over a short enough time within a material to produce detectable elastic waves or acoustic emission. Proposed mechanisms have included crack propagation, precipitate or inclusion fracture, twin formation, martensite formation, dislocation motion, and dislocation multiplication.

Measurements are reported here of the effect of nucleation and growth of precipitates during aging on acoustic emission from dislocation sources. Measurements have been made on a number of precipitation-strengthened alloys including 7075, 6061, and 2219 aluminium alloys; JBK-75 (similar to A286), KHB (an experimental alloy age hardened with a NiBe precipitate), and 17-10P stainless steels; Incoloy 903; and sterling silver. Results from 5083 aluminium, a solid-solution-strengthened alloy, are also reported. A qualitative model is proposed which predicts the divergent changes in acoustic emission observed with aging in the various alloy systems.

## MODELS FOR DISLOCATION SOURCES OF ACOUSTIC EMISSION

It is unlikely that the motion of a single dislocation can produce a strain wave large enough to be detected with current acoustic emission technology. Qualitative verification of this assertion is available by considering the dependence of acoustic emission level on strain in a typical constant crosshead velocity tensile test. In the absence of non-dislocation acoustic emission sources (such as precipitate or inclusion fracture, cracking or strain-induced phase transformations) the amount of acoustic emission generally reaches a maximum near the onset of plastic flow, and declines thereafter to small values or zero at large strains. However, the plastic strain rate and hence the amount of dislocation motion (proportional to the mobile dislocation density and their average velocity) is greater in a typical constant crosshead speed tensile or compression test at large strains than near yield. If the motion of individual dislocations were being measured, an increase in the acoustic emission from yield to at least the ultimate tensile strength would be expected rather than the observed decrease.

Some mechanism is therefore required which results in the nearly simultaneous motion of many dislocations within a small volume of the sample in order to produce detectable acoustic emission from dislocation motion. Two mechanisms satisfying this requirement have been advanced. James and Carpenter<sup>1</sup> proposed the event responsible for acoustic emission to be the nearly simultaneous breakaway of a set of pinned dislocations within a small volume of the sample. As the stress is increased on a set of pinned dislocations, one or a small

\* Prepared under Contract no. DE-AC04-76DP03533 for the Albuquerque Operations Office, US Department of Energy. Rockwell International Corporation and the US Government expressly reserve the right to print, reprint, publish, copy, vend, translate, and use any or all material contained herein.

number of the dislocations eventually break away from their pins. The small stress wave produced by the breakaway could trigger the breakaway of other pinned dislocations nearby, leading to an avalanche of moving dislocations. The consequent stress relaxation will produce a detectable elastic wave if the number of dislocations involved and the distance they travel are large enough, and if the time interval over which the motion occurs is short enough. It is not certain whether the acoustic emission arises from the breakaway of the dislocations in the avalanche from their pins, the glide of the avalanche after breakaway, the arrest of the avalanche at obstacles, or a combination of these events. Physically plausible dislocation lengths are required if the elastic wave is generated from the energy release caused by yielding of a small stressed region from dislocations passing through it, i.e. by the glide of the avalanche. The motion of 0.2 cm of dislocation line was estimated to produce an average size event in beryllium. James and Carpenter estimated that 2000 cm of dislocation line was involved in an average event in LiF. This is discussed in more detail by Carpenter and Heiple.<sup>2</sup> The avalanche need not necessarily originate from the breakaway of existing pinned dislocations. It could just as well originate from the nearly simultaneous activation of many dislocation sources within a local region, most likely grain-boundary sources triggered by a mechanism similar to that proposed for breakaway avalanches.

A second model with some features in common with the avalanche model has been advanced by Agarwal *et al.*<sup>3</sup> They proposed that, as a sample is loaded, a stress is eventually reached at which Frank-Read or grain-boundary sources are activated. The new dislocations move along the slip plane until they are stopped by an obstacle, such as a grain boundary, precipitate, or other dislocations. The source, once activated, was proposed to rapidly produce new dislocations until the back stress arising from the pile-up of the new dislocations against an obstacle became large enough to shut it off.

The Frank-Read source model predicts a reduction in acoustic emission with aging in precipitation-strengthened alloys because the precipitates reduce both the length of the Frank-Read sources and the glide distance of the newly created dislocations. Some increase in acoustic emission may occur in the overaged condition where the precipitates have become larger and more widely spaced. Agarwal *et al.*<sup>3</sup> observed precisely this behaviour in 2024 aluminium, and Schmitt-Thomas *et al.*<sup>4</sup> observed the same behaviour in an essentially identical German aluminium alloy. However, preliminary measurements in a precipitation-strengthened austenitic stainless steel showed an increase in acoustic emission with aging.<sup>2</sup> It is not clear how this increase can occur on the basis of the Frank-Read source model.

If precipitates serve as breakable pins, then they may increase the size and frequency of dislocation avalanches and lead to an increase in acoustic emission if the avalanche model is correct. On the other hand, they could simply reduce the glide distance of avalanches and thereby reduce the acoustic emission. The avalanche model therefore predicts that the details of the dislocation-precipitate interaction determine whether acoustic emission from dislocation motion is enhanced or reduced by the nucleation and growth of precipitates during aging of age-hardening alloys.

We propose that the effect of precipitates on acoustic emission from dislocation motion is governed primarily by the slip character of the material and by the size and strength of the precipitates. In alloys where cross slip is relatively easy, dislocations bypass precipitates by cross

slipping around them individually, a process unlikely to lead to dislocation avalanches. Ease of cross slip is governed mainly by the separation of partial dislocations, which is in turn directly proportional to the elastic modulus and inversely proportional to the stacking fault energy. In easy cross slip systems (high stacking fault energy, low modulus), acoustic emission should be relatively low after aging and insensitive to the size or strength of the precipitates achieved during aging. Precipitation-strengthened aluminium alloys fall into this class.

By contrast, in alloys where cross slip is more difficult, dislocations tend to pile up at precipitates and, if the precipitates are not too strong, cut through them in a way more likely to produce avalanches. In these systems (low stacking fault energy, high modulus), acoustic emission levels may be relatively high after aging and sensitive to the size and nature of the precipitates. In particular, the amount of acoustic emission observed near yield should increase with increased aging time until the precipitates become strong enough, so that they begin to no longer serve as breakable pins, at which point the amount of observed emission should decrease. Precipitation-strengthened austenitic stainless steels fall into this class.

If the breakable pins are Cottrell atmospheres instead of precipitates, then slip character should have little effect on the amount of acoustic emission produced. Cottrell atmospheres are known to provide breakable pinning of dislocations under certain conditions, as for example when Portevin-Le Chatelier (serrated) yielding occurs or in many cases when load drops are produced at yield. Substantial acoustic emission would therefore be expected in both easy and difficult cross slip systems when yield points or serrated yielding is observed. Furthermore, precipitation removes material from solid solution, thus acoustic emission may be reduced during aging in some systems simply by reducing the pinning of dislocations by Cottrell atmospheres.

Stacking fault energy has been investigated previously as a material parameter influencing acoustic emission behaviour. Imaeda *et al.*<sup>5</sup> found no consistent correlation between the rms peak height near yield and stacking fault energy for several pure fcc metals; however, Hatano<sup>6</sup> reported that the amount of observed acoustic emission decreased with lower stacking fault energy for a different set of fcc metals and alloys.

## EXPERIMENTAL

### Acoustic emission measurements and mechanical testing details

Acoustic emission was detected during tensile and compression tests with a Dunegan-Endevco (D/E) S140 transducer, which is a PZT-5A piezoelectric, longitudinally resonant type transducer with a 140 kHz resonant frequency. The transducer was located on the gauge section of the samples and was coupled to the sample with a viscous resin (Dow 276-V9). The output of the transducer was amplified with a Panametrics model 5050AE-160A preamplifier (tests on Incoloy 903 used a D/E model 802P preamplifier) and fed into a D/E model 301 totalizer with a frequency bandpass of 100-300 kHz. Measurements were generally made with a system gain of 110 dB (85 dB for Incoloy 903). The amplified bandpassed signal was measured with a Hewlett Packard 3400A rms voltmeter and monitored with an oscilloscope.

Deformation of the tensile and compression samples was produced by a universal testing machine with a screw-driven crosshead at a nominally constant crosshead speed of 0.05 mm min<sup>-1</sup>. The load on the sample was obtained from the testing machine load cell. Sample deformation was

**Table 1** Average strain rate at rms peak near yield for alloys tested

Alloy	Strain rate, min <sup>-1</sup>	Approximate deforming volume, cm <sup>3</sup>
2219 Al	0.0010	0.25
6061 Al	0.0005-0.0013*	0.25
7075 Al	0.0011	0.25
5083 Al	0.0023†	0.25
JBK-75	0.0004-0.0012*	0.25
KHB	0.0007	0.72
Incoloy 903	0.0003†	0.55
17-10P	No peak	0.25
Ag-7Cu	0.0012	0.25

\* Varied with heat treatment.

† Estimated from load-time curves.

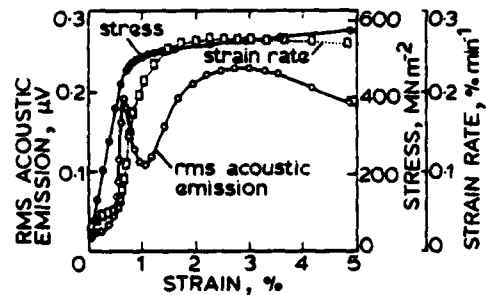
measured with a 0.5 in, 10% extensometer attached to the tensile bar gauge section (or the compression platens). For the Incoloy 903 tests, sample deformation was calculated from the load-time curve, with testing machine deformation subtracted.

Outputs from the rms voltmeter, load cell, and extensometer were all recorded on strip chart recorders, yielding a record of all these parameters v. time. Stress and rms voltage were then replotted from these data v. strain. Noise was subtracted from the measured rms acoustic emission using the relation  $V_{rms}^2 = rms_m^2 - rms_n^2$ , where  $V_{rms}$  is the actual acoustic emission output voltage,  $rms_m$  is the measured rms acoustic emission voltage, and  $rms_n$  is the rms noise voltage.<sup>7</sup>

The tensile bars used for most of the tests had a circular cross-section 4 mm diameter with a 1.9 mm reduced section and threaded ends. This tensile bar is one of the small-size round tension test specimens proportional to the ASTM standard round specimen (see Fig. 8 of Ref. 8). Tension samples for testing KHB and Incoloy 903 were pin-loaded sheet-type specimens which were also essentially subsize versions of the standard pin-loaded tension test specimen (see Fig. 7 of Ref. 8) and had a reduced section of ~2.5 cm. The grips of all tensile samples were preloaded to at least 150% of the expected ultimate load before testing, so that acoustic emission from the grips during the actual test would be reduced.

The measure of acoustic emission reported here is the rms voltage output of the acoustic emission transducer. It is generally believed to be proportional to the square root of the volume of the portion of the sample which is deforming. The deforming volume differed for the different tensile bar geometries employed; the approximate reduced section volumes for tensile bars used for the various alloys are given in Table 1.

The rms voltage is also believed to be proportional to the square root of the strain rate, provided the acoustic emission mechanism is not affected by a change in strain rate. A review of evidence on the effect of strain rate and sample volume on acoustic emission is given by Carpenter and Heiple.<sup>2</sup> Unfortunately, the strain rate in a nominally constant crosshead velocity test is not constant. The sample stiffness (slope of the sample load-length curve) changes drastically after plastic flow begins, and thus the distribution of crosshead displacement between sample deformation and elastic deformation of the testing machine changes. A plot of measured strain rate and stress v. strain for a 7075 aluminium sample is given in Fig. 1. In addition, the sample stiffness varies with material and sample

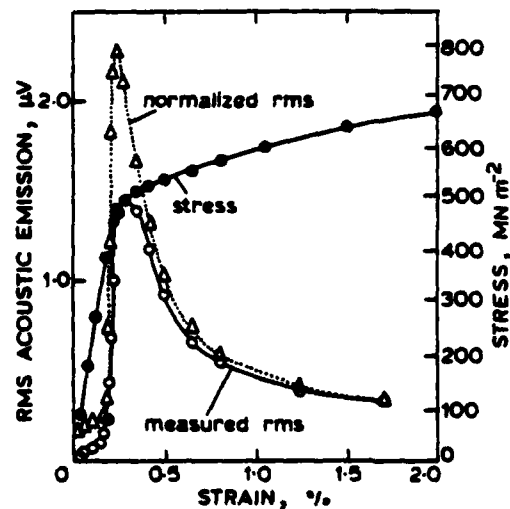


1 Acoustic emission (referred to transducer output and corrected for noise), stress, and strain rate for 7075 aluminium tensile bar aged 1 h at 120°C

geometry, which leads to different strain rates for different materials even with the same tensile bar geometry.

The rms peak located near the onset of plastic flow occurs at small plastic strains, generally less than the 0.2% plastic strain used to define the yield stress. As can be seen from Fig. 1, this is the portion of the stress-strain curve where the strain rate is changing most rapidly. It is also apparent from Fig. 1 that a small change in the location of the peak relative to the elastic limit will result in a significant difference in the actual strain rate at the location of the rms peak. A shift in peak location with heat treatment and a consequent change in strain rate at the rms peak was observed in JBK-75 and 6061 aluminium, but not in KHB or 7075 aluminium. Small changes in peak location occurred in sterling silver and 2219 aluminium, but no peak was observed in 17-10P, and extensometer-derived strain-rate data were not available for Incoloy 903.

The rms data can be normalized to a constant strain rate and constant volume to compensate for strain rate and sample size variations if it is assumed that rms is proportional to the square root of both strain rate and sample volume. A normalized rms plot v. strain is compared to an as-measured rms curve in Fig. 2 for JBK-75. The rms peak



2 Acoustic emission (referred to transducer output and corrected for noise), normalized acoustic emission, and stress for JBK-75 tensile bar from set 2 aged 4 h at 720°C; normalized rms curve was prepared by multiplying measured rms at each strain  $\epsilon$  by  $\sqrt{0.0019/t(\epsilon)}$ , where 0.0019 was strain rate at 1.7% strain and  $t(\epsilon)$  is strain rate at strain  $\epsilon$  (see Table 5 for details of specimen heat treatment)

**Table 2** Nominal composition of commercial aluminium alloys

Alloy	Element, wt.-%									
	Si	Mn	Cr	Al	Cu	Ti	V	Zr	Mg	Zn
2219	..	0.3	..	Balance	6.3	0.06	0.1	0.18	..	..
6061	0.6	..	0.2	Balance	0.28	..	..	..	1.0	..
7075	..	..	0.23	Balance	1.6	..	..	..	2.5	5.6
5083	..	0.7	0.15	Balance	..	..	..	..	4.4	..

heights for JBK-75 and 6061 aluminium as a function of heat treatment normalized to a constant strain rate at the peak are included in addition to the as-measured peak heights in the results presented subsequently. The difference between the normalized and as-measured rms peak heights v. heat treatment was small for the other alloys and the normalized peak heights are not included. The average strain rates at the rms peak for the alloys tested are given in Table 1.

#### Materials tested: aluminium alloys

The literature on the aluminium alloys tested is vast. The summary which follows is, of necessity, brief; a more extensive summary with complete references to the original literature is available elsewhere.<sup>9,10</sup> It should be noted that commercial aluminium alloys contain impurities in addition to intentional additives. In commercial 7075, for example, iron- and silicon-rich inclusions represent ~1.3 vol.-% of the material.<sup>11</sup>

#### 2219 aluminium

The nominal composition of 2219 is given in Table 2. It is essentially a binary aluminium-copper alloy with Mn, Zr, and V additions to raise the recrystallization temperature, retard grain growth, and improve the high-temperature properties. About two-thirds of the manganese should be in solid solution with the remainder as  $\text{Cu}_2\text{Mn}_3\text{Al}_{20}$ . Titanium is added as a grain refiner. After solution heat treatment there is rapid nucleation and growth of Guinier-Preston GP (1) zones at room temperature. These zones consist of layers of copper 1-2 atoms thick interspersed with layers of nearly pure aluminium. The disc-shaped GP (1) zones are coherent with the aluminium matrix and reach a diameter of 100-150 Å. Strengthening is believed to arise from lattice

distortion and interference with dislocation motion. Above ~80°C the GP (1) zones are replaced in time by GP (2) zones, also known as  $\theta'$ -zones. These disc-shaped zones have diameters of 100-1000 Å, thicknesses of 10-40 Å, and are coherent with the aluminium lattice. Maximum strength in 2219 occurs upon complete development of GP (2) zones. Aging above ~225°C will convert the GP (2) zones into  $\theta'$ , a transitional structure of  $\text{CuAl}_2$ . The  $\theta'$ -discs are incoherent (possibly semicoherent), 100-6000 Å in diameter, and 100-150 Å thick. The formation of  $\theta'$  results in softening of the alloy. Above ~275°C  $\theta'$  is converted into equilibrium  $\text{CuAl}_2$ , or  $\theta$ -phase. This phase is also incoherent. The heat treatments used in this study are given in Table 3 along with the predominant precipitate anticipated for each heat treatment.

#### 6061 aluminium

The nominal composition of 6061 is given in Table 2. It is an aluminium-magnesium-silicon alloy with the magnesium-silicon content balanced to approximately the ratio found in the equilibrium precipitate  $\text{Mg}_2\text{Si}$ . Chromium and copper are added for solid-solution strength, and the Cr also inhibits grain growth. The initial precipitates at room temperature after solution heat treatment are spherical Guinier-Preston zones. These quickly grow into needle-like shape, 15-60 Å in diameter and 160-2000 Å long. With continued aging the needles coarsen into ordered  $\text{Mg}_2\text{Si}$  rods. The rods eventually grow into platelets of  $\text{Mg}_2\text{Si}$ . Maximum strength occurs just before platelet formation begins. The heat treatments used in this study are given in Table 3 along with the predominant precipitate anticipated for each heat treatment.

#### 7075 aluminium

The nominal composition of 7075 is given in Table 2. It is an aluminium-copper-magnesium-zinc alloy. Chromium is added to improve resistance to stress corrosion cracking. The alloy contains a moderate excess of magnesium over that needed to form the equilibrium  $\text{MgZn}_2$  precipitate. The copper provides solid-solution strengthening and also substitutes for zinc in the transition and precipitate phases. Copper does not appear to have a major effect on the precipitation process.

**Table 3** Heat treatments for commercial aluminium alloys

Alloy	Solution treatment*	Aging treatment	Temper designation	Predominant precipitate expected
2219	550°C, 1.5 h	20°C, > 96 h	T4	GP (1)
	550°C, 1.5 h	20°C, > 96 h; 190°C, 30 h	T62	GP (2)
	550°C, 1.5 h	20°C, > 96 h; 250°C, 48 h	Overaged	$\theta'$
	550°C, 1.5 h	415°C, 1 h; cool $\leq 25 \text{ K h}^{-1}$	O	$\theta$
6061	545°C, 15-20 min	-78°C, < 2 h	..	None
	545°C, 15-20 min	20°C, ~ 6 months	..	GP needles
	545°C, 15-20 min	175°C, 1 h	..	GP needles
	545°C, 15-20 min	175°C, 4 h	..	$\text{Mg}_2\text{Si}$ rods
	545°C, 15-20 min	175°C, 8 h	T6	$\text{Mg}_2\text{Si}$ rods
	545°C, 15-20 min	205°C, 24 h	Overaged	$\text{Mg}_2\text{Si}$ platelets
	545°C, 15-20 min	-78°C, < 2 h	..	None
7075	482°C, 15-20 min	120°C, 1 h	..	GP spheres
	482°C, 15-20 min	120°C, 8 h	..	GP spheres
	482°C, 15-20 min	120°C, 25 h	T6	GP spheres
	482°C, 15-20 min	175°C, 8 h	~ T73	M' and/or M $\text{MgZn}_2$
	482°C, 15-20 min	415°C, 1 h; cool $\leq 25 \text{ K h}^{-1}$	O	$\beta\text{-Mg}_2\text{Al}_3$

\* All samples water quenched after solution heat treatment.

The initial precipitates at room temperature after solution heat treatment are spherical GP zones with a 20–30 Å diameter. Aging below ~130°C for short times alters the GP zone diameter little. Maximum strength is achieved at the maximum density of these GP zones. As aging continues, the spheres coarsen into plates with about the same thickness as the spheres. Further aging converts the GP plates into partially coherent  $M'$   $MgZn_2$  and eventually into equilibrium  $M$   $MgZn_2$ . The heat treatments used in this study are given in Table 3 along with the predominant precipitate anticipated for each heat treatment.

#### 5083 aluminium

The nominal composition of 5083 is given in Table 2. The alloy is solid-solution strengthened with magnesium; there is, however, a considerable excess of magnesium above the 1.9% which can be in equilibrium solid solution at room temperature. The excess magnesium precipitates very rapidly after quenching from elevated temperature as spherical GP zones of 10–15 Å diameter. These GP zones provide negligible strengthening. If the alloy is heated above 50–70°C the GP zones are replaced by coherent  $\beta'$ - $Mg_3Al_2$ , primarily located at grain boundaries. (The  $\beta'$  forms directly if the alloy is quenched to a temperature above 50–70°C.) With longer times the  $\beta'$  is converted to incoherent  $\beta$ - $Mg_3Al_2$ ;  $\beta$  forms directly from the matrix above 275°C. The Mn and Cr additions retard formation of the GP zones and accelerate  $\beta'$ -formation. The only heat treatment reported in this investigation is the 'O' condition, as indicated in Table 3.

#### Materials tested: iron-base alloys

##### JBK-75 austenitic stainless steel

Alloy JBK-75 is an age-hardenable austenitic stainless steel, similar to commercial A286, but with chemistry modifications to improve resistance to hot cracking during welding.<sup>12,13</sup> The primary modifications are an increase in nickel and a decrease in manganese, carbon, phosphorus, sulphur, silicon, and boron. The composition range for JBK-75 is given in Table 4. Alloy A286 was one of the early superalloys and many of the alloying elements are designed to improve its high-temperature performance.

Age hardening is achieved by precipitation of  $\gamma'$ - $[Ni_3(Ti, Al)]$  after solution heat treatment.<sup>11</sup> The  $\gamma'$  precipitates as spherical coherent particles in the range 500–850°C. The  $\gamma'$ -precipitates grow with increased aging time

Table 4 Composition of iron-base alloys

Element, wt.-%	Alloy			
	JBK-75	KHB, heat 5	Incoloy 903	17-10P
C	0.01–0.03	0.027–0.058	0.03	0.12
Si	0.20 max.	0.3	0.07	0.61
Mn	0.30 max.	0.2	0.15	0.81
P	0.010 max.	..	..	0.25
S	0.010 max.	..	0.004	0.016
Cr	13.5–16	20	..	16.8
Mo	1.0–1.5	0.01	..	0.11
Ni	29.0–31.0	30.5	37.5	10.4
Al	0.15–0.35	0.01	1.0	..
B	0.001 max.	..	..	..
Co	..	0.05	15.3	0.16
Nb + Ta	..	..	2.8	..
Ti	2.0–2.3	0.07	1.4	..
V	0.1–0.5	..	..	..
Be	..	0.44	..	..
Fe	Balance	Balance	Balance	Balance

Table 5 Heat treatments used for iron-base alloys

Alloy	Solution treatment*	Aging treatment	Predominant precipitate expected
JBK-75	985°C, 1 h, He quench	Set 1†: none	None
		Set 1: 675°C, 0.5, 1, 4, 16, 64 h	$\gamma'$
	985°C, 1 h, He quench	Set 2†: 720°C, 0.5, 1, 2, 4, 16, 64, 256 h	$\gamma', \eta$ at 16 or more h
KHB	1150°C, 1 h	Set 3: none	None
		Set 3: 720°C, 1, 4, 16, 64, 256 h	$\gamma', \eta$ at 16 or more h
Incoloy 903	980°C, 1 h	500°C, 0.5, 1, 2, 4, 8, 16, 32, 72 h	GP zones only
		600°C, 0.5, 1, 2, 4, 8, 16, 32, 72 h	GP zones initially, $\beta'$ after 1–4 h
17-10P	980°C, 1 h	None	None
		720°C, 8 h, cool at 100 K h <sup>-1</sup> to 620°C, hold 8 h	$\gamma'$
	1120°C, 0.5 h	720°C, 16 h	$\gamma'$
		None	None
	1120°C, 0.5 h	705°C, 1, 2, 4, 8, 16, 32 h	$M_{23}C_6$

\* Except as noted, all samples water quenched after solution heat treatment and aging treatment.

† Sets 1 and 2 homogenized 4 h at 1205°C and cold swaged 62% before solution treatment.

and provide increased strength. Overaging leads to conversion of the  $\gamma'$  into the equilibrium  $\eta$ - $(Ni_3Ti)$ , which usually forms a cellular precipitate and generally nucleates at grain boundaries. Formation of optically observable  $\eta$  begins well before maximum strength is achieved by aging. As would be expected from the complex nature of the alloy, a number of other minor phases have been reported.<sup>14</sup> The heat treatments and expected precipitates for this study are given in Table 5.

##### KHB austenitic stainless steel

The KHB alloy is an experimental austenitic stainless steel which resulted from an effort to make a useful engineering alloy from beryllium-contaminated type 304L stainless steel scrap. Substantial nickel additions to 304L were required to maintain an austenitic structure because beryllium is a powerful ferrite stabilizer. The composition of experimental heat 5, which was used for the work reported here, is given in Table 4. The alloy is single-phase austenite after solution heat treatment at 1150°C followed by a water quench. The initial precipitates during aging between 500 and 600°C are coherent disc-shaped GP zones. At 600°C and above, these GP zones grow into semicoherent disc-like  $\beta'$ - $(NiBe)$ . Aging at higher temperatures will convert the  $\beta'$  to incoherent  $\beta$ - $(NiBe)$ .<sup>15</sup> The precipitation reactions will be discussed in more detail in the section headed 'Results'. The heat treatments used for this investigation are given in Table 5.

##### Incoloy 903

Incoloy 903 is an age-hardenable iron-nickel-cobalt-base superalloy. The matrix is austenite and the hardening precipitate is  $\gamma'$ - $[Ni_3(Ti, Al)]$ . The composition is given in Table 4. The alloy is single phase after solution heat treatment. The aging treatment for optimum mechanical properties according to the producer's recommendations is a dual aging treatment at 720 and 620°C, which produces cuboidal coherent  $\gamma'$ -particles of order 175 Å on a side.

These particles grow with increased aging time.<sup>16</sup> The heat treatments used in this study are given in Table 5.

#### 17-10P stainless steel

The 17-10P alloy is an age-hardenable austenitic stainless steel. It is no longer commercially available in laboratory quantities; however, Armco Research Laboratories generously provided the authors with a 30 lb experimental casting for this investigation, the analysis of which is given in Table 4. The casting was redundantly forged ~35% at 1120°C, water quenched, homogenized for 24 h at 1120°C, furnace cooled, and rolled in several passes with intermediate reheats at 1120°C. The total rolling reduction was ~85%. Samples were cut from the plate after the hot breakdown and heat treated. Heat treatments used are given in Table 5.

We have been unable to locate specific reference to precipitation processes in 17-10P, but there have been a number of investigations of high-phosphorus-high-carbon austenitic stainless steels.<sup>17-20</sup> On the basis of these investigations it appears that the hardening precipitate is a finely dispersed  $M_{23}C_6$  type carbide with chromium being the major metal in the carbide. The role of phosphorus is to aid in the precipitation of the finely dispersed carbide. It should be noted that carbides differ from the hardening precipitates in the other alloys studied. Carbides are hard and are not expected to be cut by dislocations.

#### Materials tested: sterling silver

The silver-copper equilibrium phase diagram is of the simple eutectic type with fairly restricted terminal solid solutions and no intermediate phases. The solid solubility of copper in silver decreases from 8.8 wt-% copper at the eutectic temperature (779°C) to ~0.2% at 100°C (Ref. 21). The alloy tested contained ~7% copper. The equilibrium precipitate for alloys near this composition is a solid solution of silver in copper which forms by cellular precipitation starting at grain boundaries. However, Gust et al.<sup>22</sup> have shown the existence of two metastable precipitate phases on the basis of hardness measurements which form from the solid solution upon aging.

The alloy had a cast structure with evidence of fairly severe copper segregation. Nevertheless, substantial strengthening occurred during aging of solution heat-treated samples, although aging times required were longer than would be expected in homogeneous wrought material. Heat treatments employed are given in Table 6.

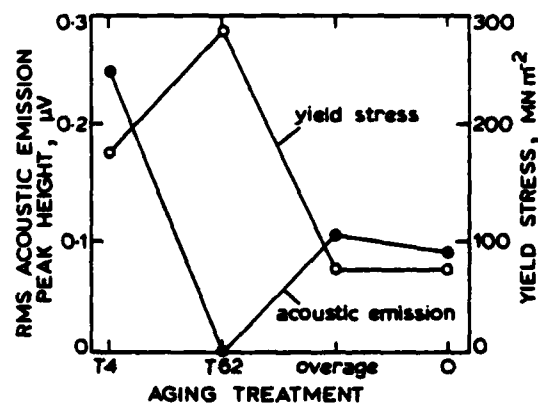
#### RESULTS

The alloys tested have been grouped according to slip character. The easy cross slip alloys include the aluminium alloys, which all have high stacking fault energies and low elastic moduli. Sterling silver is also placed in this group even though it has a low stacking fault energy. The stacking fault energy of silver (22 erg  $\text{cm}^{-2}$ ) may be lowered by the copper added to make the alloy.<sup>23</sup> Sterling silver also has a low elastic modulus, so cross slip should be easier than in

Table 6 Heat treatments for sterling silver

Material	Solution treatment	Aging treatment
Ag-7Cu*	720°C, 30 min	None
	720°C, 30 min	535°C, 45 min
	720°C, 30 min	535°C, 170 min

\* Water quenched from each heat treatment step.



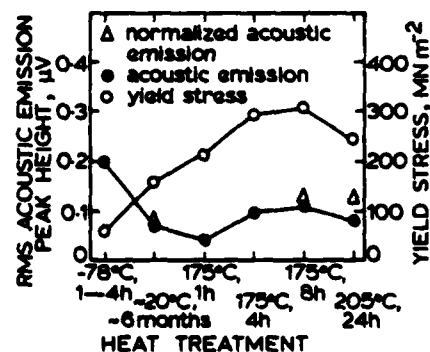
3 Yield stress (0.2%) and magnitude (referred to transducer output and corrected for noise) of rms acoustic emission peak near onset of plastic flow in 2219 aluminium as function of aging treatment

the iron-base alloys tested, even though they have higher stacking fault energies.

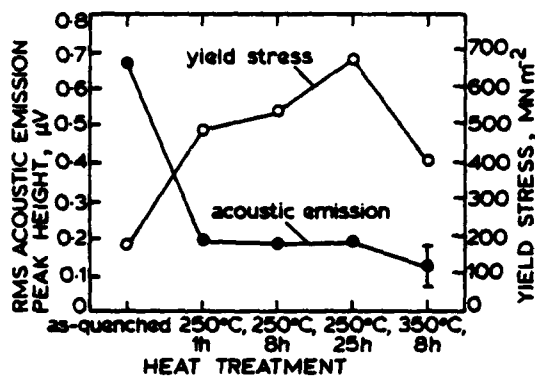
The stainless steels (except 17-10P) and Incoloy 903 are grouped together as moderately difficult cross slip systems. All these alloys have similar elastic moduli (about three times that of aluminium). The stacking fault energy, estimated from Fig. 8 of Ref. 24, is 35 erg  $\text{cm}^{-2}$  for KHB and 50 erg  $\text{cm}^{-2}$  for JBK-75. This value for JBK-75 is probably ~10 erg  $\text{cm}^{-2}$  too high, since ~10 wt-% nickel is removed from solution by precipitation, which would leave a predicted stacking fault energy of 40 erg  $\text{cm}^{-2}$ . Slip in JBK-75 hardened with ordered coherent  $\gamma'$  has been shown to be planar for small strains with the dislocations cutting the  $\gamma'$ -particles.<sup>14</sup> The same reduction of nickel in solution occurs in KHB but the composition is such that there is little effect on stacking fault energy. No estimate for the stacking fault energy of Incoloy 903 was found.

The 17-10P alloy is classed as a difficult cross slip system. It has an elastic modulus equivalent to that of the iron-base alloys and an estimated stacking fault energy (see Fig. 8 of Ref. 24) of 18 erg  $\text{cm}^{-2}$ .

The acoustic emission measurements reported here are for the acoustic emission peak near the onset of plastic flow. This peak has been shown by a variety of tests to arise from



4 Yield stress (0.2%) and magnitude (referred to transducer output and corrected for noise) of rms acoustic emission peak near onset of plastic flow in 6061 aluminium as function of heat treatment: normalized peak heights are also plotted, as-measured peak heights were normalized to strain rate of 0.00128  $\text{min}^{-1}$ , which was measured strain rate at peak for samples aged 4 h at 175°C



5 Yield stress (0.2%) and magnitude (referred to transducer output and corrected for noise) of rms acoustic emission peak near onset of plastic flow in 7075 aluminium as function of heat treatment; uncertainty in peak height after aging 8 h at 350°C is due to overlap of peak near yield by another peak centred at  $\sim 1.6\%$  plastic strain

dislocation motion in beryllium<sup>25,26</sup> and in 7075 aluminium.<sup>27</sup> A second peak centred beyond 1% plastic strain is also observed in a number of the alloys tested, including three aluminium alloys (2219, 6061, and 7075). An example of the rms acoustic emission from 7075 is shown in Fig. 1. The second peak in 7075 has been associated with inclusion fracture and/or debonding.<sup>27</sup> The origin of the second peak in 2219 and 6061 is likely to be the same since the inclusion content is comparable to 7075.

#### Easy cross slip systems

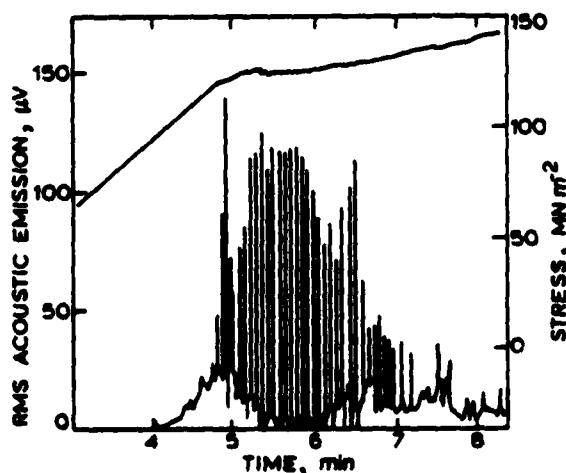
The 0.2% yield stress and the magnitude of the rms acoustic emission peak at the onset of plastic flow in 2219 aluminium are shown in Fig. 3 as a function of heat treatment. Results for 6061 aluminium are plotted in Fig. 4 and for 7075 aluminium in Fig. 5. Details of the heat treatments are given in Table 3. For 2219, the acoustic emission peak at yield was too small to detect near the maximum strength condition and is small for the other heat treatments tested.

More extensive measurements of acoustic emission as a function of aging have been reported for the German alloy AlCu4.3 by Schmitt-Thomas *et al.*<sup>28</sup> The composition of this alloy is not given in Ref. 28; however, it appears to be a binary aluminium-copper alloy containing 4.3 wt-% copper. The sequence of precipitates formed during aging is the same as in 2219. When AlCu4.3 is heated to the aging temperature after solution heat treatment and held at room temperature for 10 days, the GP (1) zones formed at room temperature redissolve and then re-form as aging continues. Schmitt-Thomas *et al.* observed an increase in the acoustic emission peak height near yield in samples in which this reversion had occurred, with a sharp drop in peak height for samples which had been aged long enough for the GP (1) zones to re-form. They also observed an increase in peak height with mild overaging followed by a decline for severe overaging. Measurements reported here for 2219 aluminium are consistent with the behaviour reported for AlCu4.3; however, no tests were made for aging conditions which would produce reversion in 2219. Acoustic emission behaviour similar to 2219 has been reported in 2024 aluminium<sup>3</sup> and AlCuMg2 (essentially identical to 2024; Ref. 4). The 2024 alloy is an aluminium-copper-magnesium alloy rather than a binary aluminium-copper alloy.

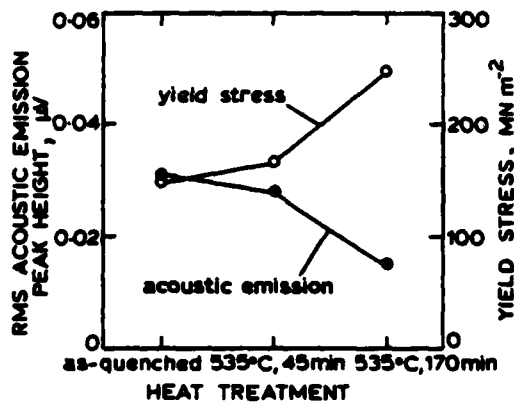
The acoustic emission peak at the onset of plastic flow is

small for all heat treatments of 6061 tested; there are small variations with aging treatment except that the peak in the solution-treated and quenched condition was about twice as large as after the other heat treatments. In contrast to 2219, the peak is not of minimum size at or near the maximum strength condition. The peak shifted to smaller plastic strains for long aging times. The peak height normalized to a constant strain rate is also plotted in Fig. 4. The corresponding peak in 7075 is also small and nearly independent of aging treatment, except that it is also substantially larger in the solutionized and quenched condition. Significant aging occurs in both 6061 and 7075 aluminium at room temperature. The solution-treated condition was retained by storing the samples in dry ice after quenching and testing within 4 h. The peak is not of minimum size at or near the maximum strength condition. Measurements by Wells<sup>29</sup> have also shown the acoustic emission peak at yield in 7075 to be largest in the solutionized and quenched condition, and to decrease with aging.

Acoustic emission from 5083 aluminium has been reported elsewhere.<sup>30</sup> The onset of plastic flow in the O condition was characterized by a load drop and a short region of serrated yielding immediately following the load drop when the same strain rate was used as in tests of the other aluminium alloys. The load and rms acoustic emission voltage are plotted *v.* time near the yield point in Fig. 6. The rms spikes associated with the Portevin-Le Chatelier load drops make a determination of the average acoustic emission levels attained near yield in 5083 difficult. Testing at crosshead speeds 5 and 10 times greater than the crosshead speed normally used essentially eliminates the serrated yielding and produces reasonably smooth rms acoustic emission peaks near yield. Their magnitudes are  $\sim 85$  and  $130 \mu\text{V}$  at crosshead speeds of 0.010 and 0.020 in  $\text{min}^{-1}$  respectively. The rms level is proportional to the square root of strain rate provided the deformation mechanism is unaffected by strain rate,<sup>2</sup> so these peak heights would correspond to  $\sim 40 \mu\text{V}$  at the normal 0.002 in  $\text{min}^{-1}$  crosshead speed. This level is two orders of magnitude larger than the peaks observed in the age-hardening aluminium alloys. The actual rms levels achieved during serrated yielding at the usual crosshead speed are even larger.



6 Rms acoustic emission (referred to transducer output but not corrected for noise) and stress *v.* time near yield for 5083 aluminium; average strain rate after yield was  $\sim 0.0023 \text{ min}^{-1}$ ; plastic strain included in figure is from zero to  $\sim 0.6\%$

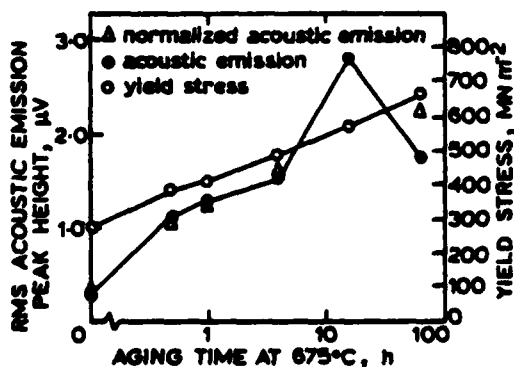


7 Yield stress (0.2%) and magnitude (referred to transducer output and corrected for noise) of rms acoustic emission peak near onset of plastic flow in sterling silver as function of heat treatment

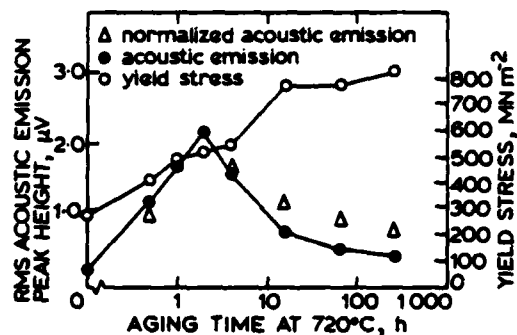
The magnitude of the rms acoustic emission peak at the onset of plastic flow in sterling silver (Ag-7Cu) is plotted in Fig. 7 for the three heat treatments tested. Only enough material for three tensile bars (one for each heat treatment) was available. Although barely detectable, the peak clearly decreased with aging. Unfortunately, the available material had a large-grained cast structure with substantial copper segregation. A number of investigators report a substantial decrease in acoustic emission with increasing grain size; however, about an equal number report an increase in acoustic emission.<sup>2</sup> Thus the effect of grain size is in doubt, but it is at least possible that the low acoustic emission level in the silver samples is due in part to the large grain size.

**Moderately difficult cross slip systems**

The magnitude of the rms acoustic emission peak at the onset of plastic flow in JBK-75 stainless steel is shown as a function of aging time in Figs. 8-10. (A plot of rms v. strain for a JBK-75 tensile bar is given in Fig. 2.) The difference between set 2 (Fig. 9) and set 3 (Fig. 10) is that set 2 received a homogenization anneal and set 3 did not; see



8 Yield stress (0.2%) and magnitude (referred to transducer output and corrected for noise) of rms acoustic emission peak near onset of plastic flow in JBK-75 as function of aging time; normalized peak heights are also plotted, as-measured peak heights were normalized to strain rate of 0.00128 min<sup>-1</sup> which was measured strain rate at peak for samples aged 16 h

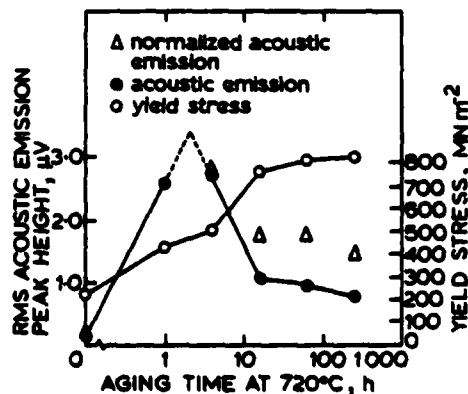


9 Yield stress (0.2%) and magnitude (referred to transducer output and corrected for noise) of rms acoustic emission peak near onset of plastic flow in JBK-75 stainless steel (set 2) as function of aging time; normalized peak heights are also plotted, as-measured peak heights were normalized to strain rate of 0.00111 min<sup>-1</sup> which was measured strain rate at peak for samples aged 2 h

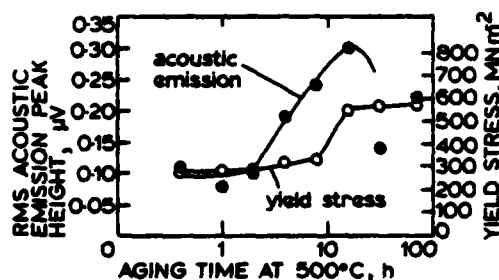
Table 5 for details of the heat treatments. The amount of acoustic emission near yield increases sharply with aging time and then declines. The maximum amount of acoustic emission occurs at aging times considerably less than those which produce maximum strength. There was a shift in the location of the rms peak toward smaller plastic strains for aging times longer than required to yield the largest acoustic emission peak. The shift to lower plastic strains resulted in a smaller strain rate at the peak for these samples, as discussed above (see Fig. 1). The peak height normalized to a constant strain rate is also plotted in Figs. 8-10. Normalization increases the relative size of the acoustic emission peak for longer aged samples.

The behaviour of KHB stainless steel is very similar to JBK-75. The rms peak height at the onset of plastic flow is shown as a function of aging time in Figs. 11 and 12. Again there is an initial rise in acoustic emission with aging time, followed by a decline with further aging.

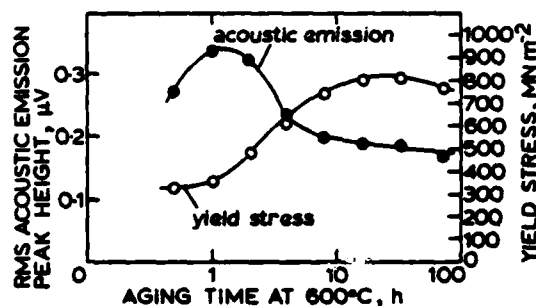
Data on the details of precipitation during aging of KHB are available as part of an effort to characterize its microstructure.<sup>15</sup> The initial precipitates to form below



10 Yield stress (0.2%) and magnitude (referred to transducer output and corrected for noise) of rms acoustic emission peak near onset of plastic flow in JBK-75 stainless steel (set 3) as function of aging time; normalized peak heights are also plotted, as-measured peak heights were normalized to strain rate of 0.00120 min<sup>-1</sup> which was measured strain rate at peak for samples aged 1 h



11 Yield stress (0.2%) and magnitude (referred to transducer output and corrected for noise) of rms acoustic emission peak near onset of plastic flow in KHB stainless steel as function of aging time



12 Yield stress (0.2%) and magnitude (referred to transducer output and corrected for noise) of rms acoustic emission peak near onset of plastic flow in KHB stainless steel as function of aging time

~ 700°C are coherent disc-shaped Guinier-Preston zones about one unit cell thick. There are three orthogonal sets of discs parallel to the austenite {100} planes. The thickness was estimated from streaking in the diffraction pattern from the zones. These are the only strengthening precipitates to form at 500°C within 900 h. The GP zones provide some strengthening as indicated in Fig. 11. At 600°C the initial GP zones begin to transform into disc-shaped semicoherent  $\beta$ -NiBe between 16 and 64 h. The  $\beta$  is coherent on the flat surfaces of the discs, but not on the edges. It is somewhat thicker, 3-5 unit cells. Development of  $\beta$  from the GP zones provides substantial additional strengthening as indicated in Fig. 12.

The changes with aging of acoustic emission at the onset of plastic flow correlate well with the observed microstructural changes. As the GP discs grow to 50-75 Å in diameter and 1-2 unit cells thick, the acoustic emission increases to a maximum. Further growth of the discs results in a lower acoustic emission peak. By the time the precipitates have reached ~100 Å in diameter (aged 4 h at 600°C or 64 h at 500°C), the acoustic emission peak observed near yield has become considerably smaller. Transmission electron micrographs of KHB for these two aging conditions are given in Fig. 13. The micrographs are essentially indistinguishable, the acoustic emission peak heights are the same (0.24  $\mu\text{V}$  for a 4 h age at 600°C or 0.22  $\mu\text{V}$  for a 72 h age at 500°C), and the yield strengths are nearly equal (607  $\text{MN m}^{-2}$  for a 4 h age at 600°C or 572  $\text{MN m}^{-2}$  for a 72 h age at 500°C).

The height of the rms acoustic emission peak at the beginning of plastic flow in Incoloy 903 is shown for three heat treatments in Fig. 14. In this alloy the height of the acoustic emission peak also increases with aging. It differs from the stainless steels tested in that the peak height increased for a mild overaging treatment compared to the aging treatment designed to produce optimum mechanical properties. The amount of emission observed was also greater than in the stainless steels.

#### Difficult cross slip system

No acoustic emission peak was detected at the beginning of plastic flow in the 17-10P stainless steel. Substantial strengthening by aging occurred, however, as indicated in Fig. 15. A modest number of large acoustic emission bursts occurred throughout the tensile tests.

The initial growth of the  $\text{M}_{23}\text{C}_6$  carbides is very rapid. After only 1 h at 705°C (the recommended aging temperature) the precipitates were roughly cuboidal and ~80 Å on a side (Fig. 13). This is comparable to the diameter of the GP discs which produced maximum

emission in KHB, but the carbides are three dimensional and are very hard.

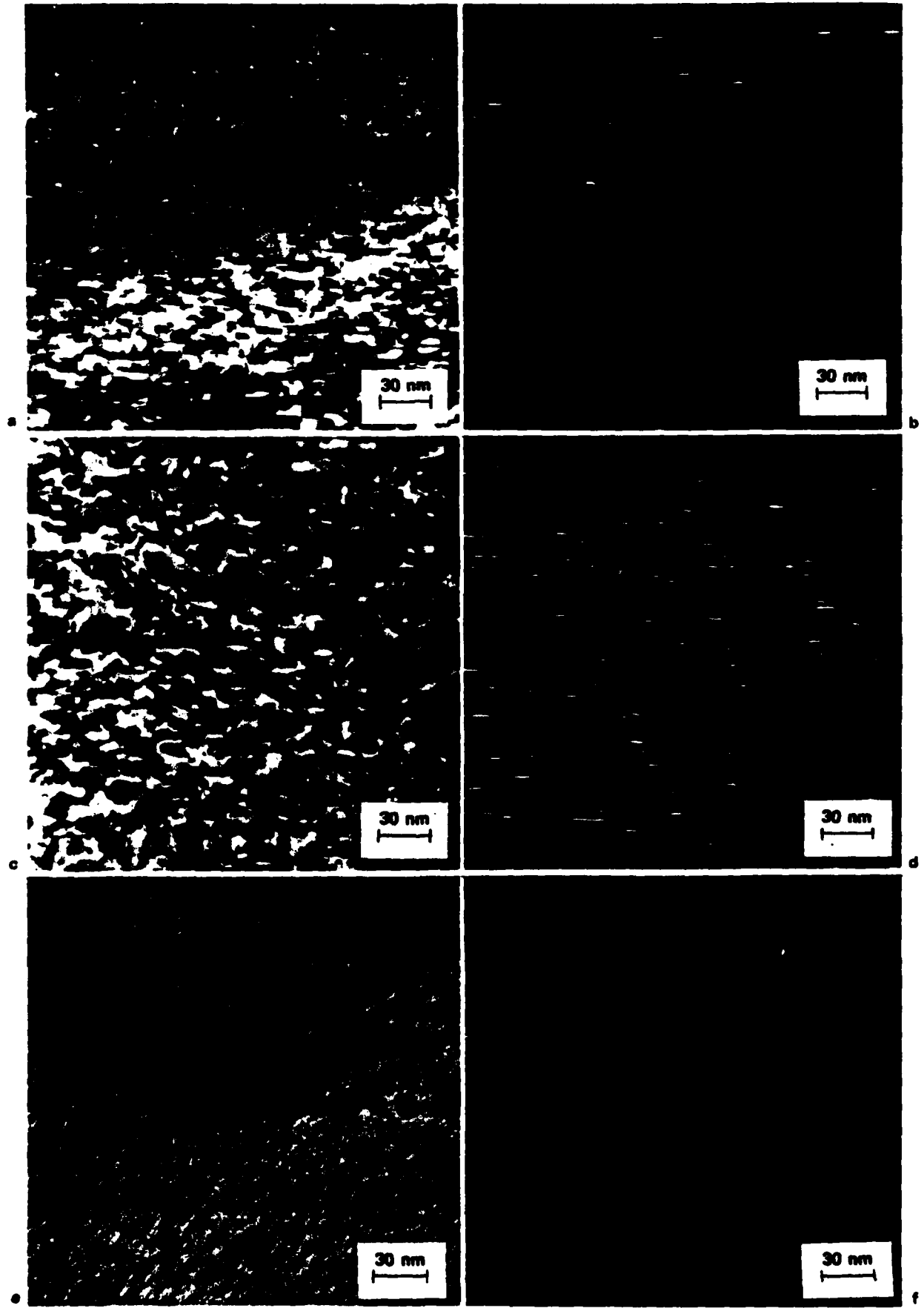
#### DISCUSSION

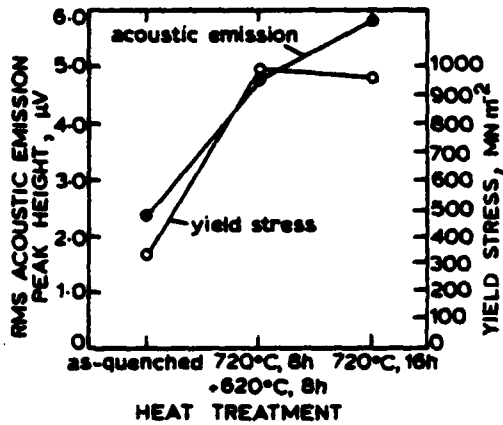
The results observed are consistent with the hypothesis that the effect of precipitation on acoustic emission is primarily governed by slip character and the strength of the precipitates. In easy cross slip systems, growth of precipitates had little effect on acoustic emission observed near yield, and the amount of acoustic emission observed was generally low. In some cases precipitate growth reduced observed acoustic emission and in others there was essentially no change. It is postulated that dislocations tend to cross slip around the precipitates and not form pile-ups which can cut through the obstacles to produce avalanches.

For moderately difficult cross slip systems, precipitation increased the amount of acoustic emission near yield. The level of acoustic emission rose as the precipitates grew, but after a certain precipitate size was achieved the amount of acoustic emission near yield decreased. (The decrease was not observed with the heat treatments used on Incoloy 903.) The levels of emission observed are generally moderate. We propose that the initial precipitates are cuttable and act as breakable pins which can serve as avalanche sites. As the precipitates grow in size and strength, they become too difficult to cut to serve as breakable pins.

It was hoped that the carbide hardening precipitates in the difficult cross slip system, 17-10P, would also serve as breakable pins. This appears not to be the case for the aging conditions tested. The carbides are already 80 Å cuboids within 1 h at the aging temperature used and are apparently uncuttable. Larger  $\gamma'$ -particles are found in Incoloy 903 for aging treatments which yield substantial acoustic emission; however  $\gamma'$ -precipitates are known to be cuttable.<sup>14,31</sup> Other aging treatments might produce breakable pins in this alloy, but a complete study of aging reactions in 17-10P was beyond the scope of this study.

When dislocations are pinned by Cottrell atmospheres, slip character should not govern the breakaway of dislocations from these atmospheres. Thus high levels of emission should be possible in easy cross slip systems which are solid-solution strengthened. Very high levels of acoustic emission were indeed observed in 5083 aluminium near yield. Furthermore, the relatively large acoustic emission peak at yield in 6061 and 7075 aluminium in the solutionized and quenched condition compared to the same alloys after aging (including room-temperature aging) can be interpreted on the same basis. In the solutionized and quenched condition, the alloying elements remain in solid solution and can provide Cottrell atmosphere pinning. Both





14 Yield stress (0.2%) and magnitude (referred to transducer output and corrected for noise) of rms acoustic emission peak near onset of plastic flow in Incoloy 903 as function of heat treatment

6061 and 7075 exhibited serrated yielding in the solutionized and quenched condition, but not after any other heat treatment. Serrated yielding is known to arise from breakaway from Cottrell atmospheres. Serrated yielding was not observed in the solutionized and quenched condition in JBK-75 or KHB and the acoustic emission was lower in this condition than after any of the aging treatments. If the reduced acoustic emission after aging 7075 and 6061 were due to restriction of avalanche glide by precipitates, a similar drop should also occur in the stainless steels. The rise in emission<sup>28</sup> at yield for aging treatments which produce reversion in AlCu4.3 may also be interpreted as arising from increased pinning by Cottrell atmospheres.

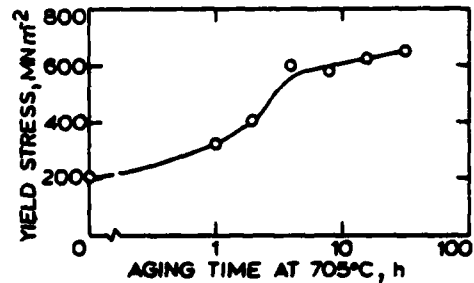
### CONCLUSIONS

A model is proposed to explain the effect of precipitation on acoustic emission from dislocation sources in age-hardening systems. The model is based on the hypothesis that a substantial number of dislocations must move rapidly and nearly simultaneously within a small volume of material in order to create detectable acoustic emission. The creation of such avalanches can be influenced by precipitation during aging. In alloy systems where cross slip is difficult, the precipitates can serve as breakable pins (if they are not too strong) which is a favourable condition for the formation of dislocation avalanches and leads to higher acoustic emission near the onset of plastic flow. In easy cross slip systems, the precipitates do not serve as breakable pins because dislocations tend to cross slip around them rather than create pile-ups. Thus precipitates should not increase acoustic emission in easy cross slip systems. These considerations do not apply if the pins are Cottrell atmospheres, and high levels of acoustic emission may be observed in easy or difficult cross slip systems when solute atmospheres provide the pinning.

Acoustic emission measurements as a function of heat treatment are reported from a variety of age-hardening

a KHB after aging 64 h at 500°C showing disc-shaped GP zones, bright field; b dark field image of a showing GP zone size; c KHB after aging 4 h at 600°C showing disc-shaped GP zones, bright field; d dark field image of c showing GP zone size; e 17-10P after aging 1 h at 705°C showing cuboidal M<sub>23</sub>C<sub>6</sub> precipitates, bright field; f dark field image of e showing carbide size

13 Transmission electron micrographs (opposite) showing precipitate size and morphology in KHB and 17-10P stainless steels



15 Yield stress (0.2%) of 17-10P stainless steel as function of aging time at 705°C

systems with various stacking fault energies and elastic moduli. Acoustic emission from aluminium alloys 7075, 6061, and 2219; iron-base alloys JBK-75, KHB, 17-10P, and Incoloy 903; and sterling silver is reported, and the acoustic emission behaviour is in agreement with the model for the effect of precipitates. A high peak of acoustic emission near yield was seen in 5083 aluminium, where serrated yielding provides evidence of pinning by solute atmospheres. Enhanced emission in 7075 and 6061 in the solutionized and quenched condition was also observed, where again serrated yielding indicated pinning by solute atmosphere.

### ACKNOWLEDGMENTS

This work was performed under Contract Number DE-AC04-76DP03533 for the US Department of Energy, Albuquerque Operations Office. Portions of this work were also supported by the National Science Foundation, Division of Materials Research, Grant Number DMR-77-23782, and the Air Force Office of Scientific Research, Division of Electronic and Solid State Sciences, Grant Number 77-3395. Their support is gratefully acknowledged. Special thanks are also given to Dr J. Arnold, Research and Technology Department, Armco Inc., and to Armco Inc., who provided us with the 17-10P stainless steel.

### REFERENCES

1. D. R. JAMES and S. H. CARPENTER: *J. Appl. Phys.*, 1971, 42, 4685-4697.
2. S. H. CARPENTER and C. R. HEIPLE: 'Fundamentals of acoustic emission', (ed. K. Ono), 49-104; 1979, Los Angeles, Calif. UCLA.
3. A. B. L. AGARWAL, J. R. FREDERICK, and D. K. FELBECK: *Metall. Trans.*, 1970, 1, 1069-1071.
4. K.-H. G. SCHMITT-THOMAS, H. M. TENSI, and H. ZEITLER: *Aluminium*, 1975, 51, 520-524.
5. H. IMAEDA, H. KUSANAGI, H. KIMURA, and H. NAKASA: Proc. Third Acoustic Emission Symp., 492-512; 1976, Tokyo, Japan Industrial Planning Association.
6. H. HATANO: *J. Appl. Phys.*, 1977, 48, 4397-4399.
7. M. A. HAMSTAD and A. K. MUKHERJEE: UCRL-76077; 1974, Livermore, Calif., Lawrence Livermore Laboratories.
8. '1979 Annual Book of ASTM Standards', Pt 10, E8-79; 1979, Philadelphia, Pa. American Society for Testing and Materials.
9. K. R. VAN HORN (ed.): 'Aluminium', Vol. 1; 1967, Metals Park, Ohio, American Society for Metals.
10. L. F. MONDOLFO: 'Aluminium alloys: structure and properties'; 1976, London, Butterworth.
11. S. M. EL-SOUDANI and R. M. PELLOUX: *Metallography*, 1973, 6, 37-64.
12. J. A. BROOKS and R. W. KRENZER: *Weld J.*, 1974, 53, 242s-245s.
13. J. A. BROOKS: *ibid.*, 517s-523s.
14. A. W. THOMPSON and J. A. BROOKS: *Metall. Trans.*, 1975, 6A, 1431-1442.

15. M. J. CARR and C. R. HEIPLE: Proc. 38th Annual Meeting Electron Microscopy Society of America, (ed. G. W. Bailey), 398-399; 1980, Baton Rouge, La. USA, Claitor's.
16. C. G. RHODES and A. W. THOMPSON: *Metall. Trans.*, 1977, 8A, 949-954.
17. A. G. ALLTEN, J. G. Y. CHOW, and A. SIMON: *Trans. ASM*, 1954, 46, 948-972.
18. B. R. BANERJEE, E. J. DULIS, and J. J. HAUSER: *ibid.*, 1968, 61, 103-109.
19. F. H. FROES, M. G. H. WELLS, and B. R. BANERJEE: *Met. Sci. J.*, 1968, 2, 232-234.
20. G. HENRY, H. G. HARDING, J. PHILIBERT, and J. PLATEAU: *Mém. Sci. Rev. Métall.*, 1967, 64, 11-21.
21. M. HANSEN: 'Constitution of binary alloys', 18-19; 1958, New York, McGraw-Hill.
22. W. GUST, B. PREDEL, and K. DIEKSTALL: *Acta Metall.*, 1978, 26, 241-245.
23. P. C. J. GALLAGHER: *Metall. Trans.*, 1970, 1, 2429-2461.
24. C. G. RHODES and A. W. THOMPSON: *ibid.*, 1977, 8A, 1901-1906.
25. C. R. HEIPLE and R. O. ADAMS: Proc. Third Acoustic Emission Symp., 342-359; 1976, Tokyo, Japan Industrial Planning Association.
26. C. R. HEIPLE and S. H. CARPENTER: Paper Summaries, ASNT National Spring Conf., 23-28; 1979, Columbus, Ohio, American Society of Nondestructive Testing.
27. S. H. CARPENTER and F. P. HIGGINS: *Metall. Trans.*, 1977, 8A, 1629-1632.
28. K.-H. G. SCHMITT-THOMAS, H. M. TENSI, and H. ZEITLER: *Aluminium*, 1977, 53, 719-723.
29. R. P. WELLS: MS thesis, 1978, University of California.
30. C. R. HEIPLE: Paper Summaries, ASNT National Fall Conf., 113-118; 1978, Columbus, Ohio, American Society of Nondestructive Testing.
31. L. M. BROWN and R. K. HAM: 'Strengthening methods in crystals', (ed. A. Kelly and R. B. Nicholson), 9-135; 1971, New York, Wiley.

## ATLAS OF HOT WORKING PROPERTIES OF THE NONFERROUS METALS:

**Volume 1: Aluminium and aluminium alloys**

**Volume 2: Copper and copper alloys**

The flow stress of metallic materials is one of the most important characteristics for the mathematical treatment of deformation processes and is the basis for all calculations of forces. Such knowledge is indispensable for scientists, for those who deal with production planning, and for all users and makers of machinery and plant.

To meet the increasing demand for characteristic deformation data, the Extrusion Committee of the Deutsche Gesellschaft für Metallkunde (DGM) has collected a set of stress-strain curves for hot working aluminium and copper and their alloys, information normally available only in numerous and widely scattered sources.

The two Atlases now available have English and German explanatory matter, and may be ordered separately. The Aluminium volume contains some 700 stress-strain curves (245 pages) and the Copper volume about 1200 (480 pages). The material is ring-bound and it is intended to issue Supplements for inclusion which will be available to subscribers at a nominal charge. Diagrams are identical in scale and dimension throughout the work to facilitate comparison. The curves are supplied with references and wherever possible methods of calculation and evaluation are described. In addition, preliminary accounts are given of experimental techniques and methods of determination, thus providing the user with a clearly arranged survey of the field.

The Metals Society has arranged with the DGM to distribute the Atlas in many areas of the world outside Germany.

**Volume 1: Aluminium and aluminium alloys**    ISBN 3-88355-000-0    320 x 265 mm  
Price: UK £36.00, post free; Overseas \$72.00, free fast post

**Volume 2: Copper and copper alloys**    ISBN 3-88355-001-9    320 x 265 mm  
Price: UK £42.00, post free; Overseas \$84.00, free fast post

Send orders with full remittance to:  
The Metals Society (MP, Sales Dept),  
1 Carlton House Terrace, London SW1Y 5DB, England.